A FEASIBILITY STUDY FOR A PORTABLE LONG PERIOD SEISMOGRAPH

by

PIERRE-MICHEL BOLDUC

B. Sc., Université Laval, 1965

A THESIS SUBMITTED IN PARTIAL FULFILLMENT OF

THE REQUIREMENTS FOR THE DEGREE OF

MASTER OF SCIENCE

in the Department

of

GEOPHYSICS

We accept this thesis as conforming to
the required standard

THE UNIVERSITY OF BRITISH COLUMBIA

June, 1971

In presenting this thesis in partial fulfilment of the requirements for an advanced degree at the University of British Columbia, I agree that the Library shall make it freely available for reference and study. I further agree that permission for extensive copying of this thesis for scholarly purposes may be granted by the Head of my Department or by his representatives. It is understood that copying or publication of this thesis for financial gain shall not be allowed without my written permission.

Department of Geophysics

The University of British Columbia
Vancouver 8, Canada

Date November 18th 1971

ABSTRACT

As a preliminary study to the operation of a portable long period seismic system, the effects of environment on the phase response of the Sprengnether 201 and Geotech SL-210 long period vertical seismometers are investigated. It is found that changes in the phase response of the seismometers are related to the zero instability of the moving mass. Pressure changes are not important in this regard; however, temperature variations should be held to less than 1°C.

Calculation of the phase response directly from the amplitude response is investigated. It is concluded that it is more practical to carry out a phase calibration directly. The technique may however be useful when only an amplitude calibration is known.

Also investigated are the noise properties of two amplifiers: the solid state Geotech AS-330 and the phototube Geotech 12613 amplifiers. The fundamental noise of the seismometer-amplifier combination is negligible. The excess noise of the AS-330 amplifier is of the same order as seismic noise at long periods at a rather noisy site.

TABLE OF CONTENTS

LIST OF FIGURES

LIST OF TABLES

ACKNOWLEDGEMENT

The author wishes to acknowledge the advice and encouragement of Dr. R. D. Russell and Dr. R. M. Ellis during the course of this research.

Special thanks are given to Dr. F. Kollar of the Earth Physics Branch, Department of Energy, Mines and Resources and Mr. Robert Meldrum for fruitful discussions on instrumentation problems.

The author would like to acknowledge also the aid of Mr. John Blenkinsop who was of great assistance in programming, Mr. Jim Misener who provided the temperature controllers and Mrs. Corinne McAdam who typed the manuscript.

Chapter I

Introduction

1.1 Background

The mechanism involved in the present models of global tectonics (Isacks et al, 1968) are not well understood. To gain insight into these mechanisms, the determination of the physical properties of the mobile regions beneath the crustal plates is of particular importance. Present data indicate that marked variations in seismic properties between regions do occur at these depths (Wickens and Pec, 1968). Regional studies are therefore required.

The optimum seismic technique presently available to investigate upper mantle properties is surface wave studies; further the costs are modest. Most previous studies have used records from permanent seismic stations. However for regional studies, portable arrays are required as the locations and spacing of permanent stations are not generally suitable.

The analytical techniques of surface wave studies are quite well developed. Using the Haskell (1953) formulation for elastic wave propagation in layered media, surface wave dispersion curves may be readily determined. For more complex geological situations, significant contributions to the theory of Rayleigh wave propagation across structural boundaries have been made by Mal and Knopoff (1965) and McGarr and Alsop (1967). Data analysis by Fourier techniques (Sato, 1955) and time variable filters (Pilant and Knopoff, 1965) are generally used with the data being fitted to models through least square inversion procedures (Dorman and Ewing, 1962).

1.2 General Problem

Studies in British Columbia would be of particular interest since we are adjacent to the ridge system of the northeast Pacific. Compared to eastern North America, it is known that the upper mantle electrical conductivities and heat flow are high and Pn amplitudes are low (Caner, 1970). On Vancouver Island, the Pn phase was not even observed in earlier explosion studies (White and Savage, 1965). This may be interpreted as a thin or missing high velocity upper mantle cap or a very thick crustal section.

For the reasons given above, the Department of Geophysics of the University of British Columbia proposes Rayleigh wave studies using data recorded by a portable tripartite array for the Vancouver Island region.

1.3 Investigations of this Thesis

For interpretation to depths much in excess of 100 km, the period of Rayleigh waves must approach 100 sec. It is well known that at these periods, temperature and pressure fluctuations and instrument noise are important factors. As portable stations must operate in adverse environments compared to that of seismic vaults, a study of these effects was considered necessary. In this thesis, a preliminary instrumentation study is carried out with the Sprengnether 201 and Geotech SL-210 long period vertical seismometers. The above considerations have lead to investigation of the following points:

(1) the effect of temperature and pressure variations in the zero stability and fundamental constants of the seismometers. (Note: Since the precision attainable in phase velocity measurements is ultimately dependent on the exact

knowledge of the phase response of the instrument, particular care is taken to relate those effects to variations in the phase response.)

(2) the noise characteristics of the solid state Geotech AS-330 (SSA) and photoelectric Geotech 12613 (PTA) amplifiers.

(3) calibration of the seismometer-amplifier-recorder system.

(4) determination of the phase response from the amplitude response.

Chapter II

The Long Period Seismometer

2.1 The La Coste Suspension

To understand the detailed behaviour of the Geotech and Sprengnether seismometers, one must understand in detail the functioning of the La Coste suspension system. This suspension consists of a boom and a mass supported by a spring and hinged so that it is free to oscillate in a vertical plane. Consider such a seismometer tilted at an angle δ and with an angle α between the mast and the boom (Fig. 1). These angles are measured positive clockwise.

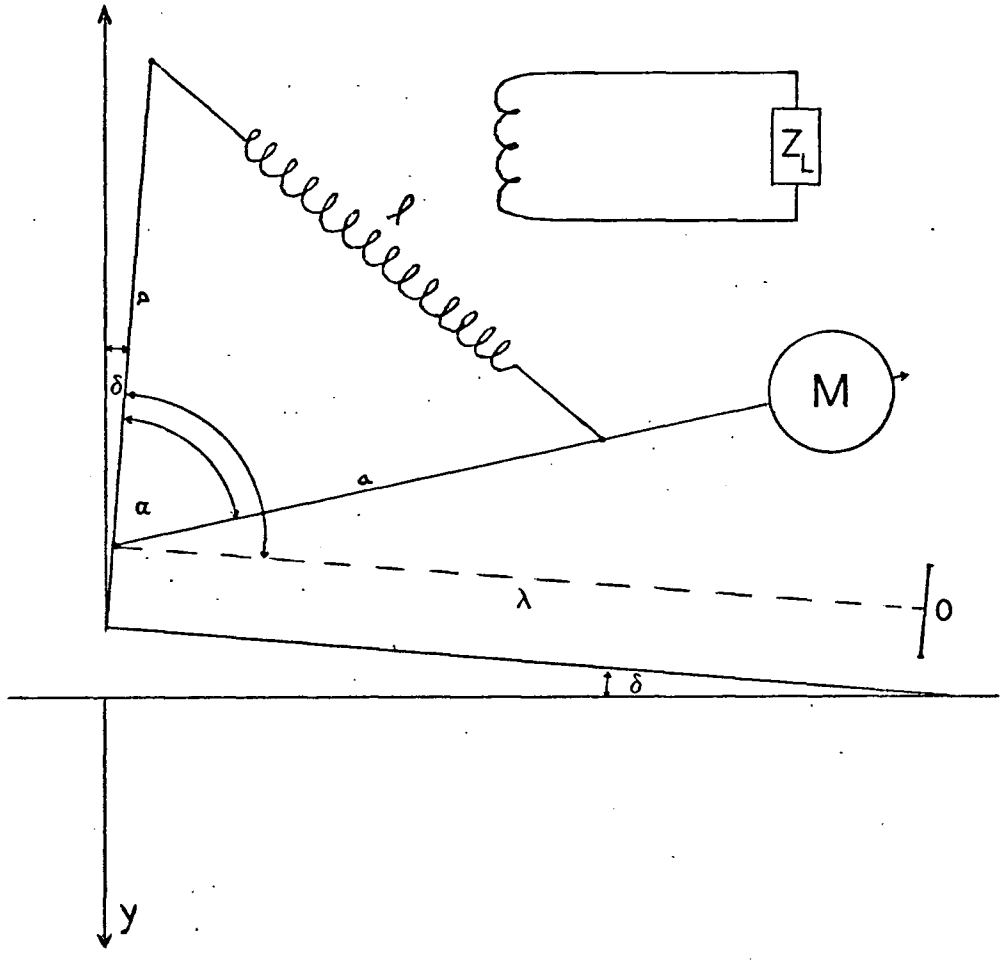

Fig. 1 Geometry of the La Coste suspension

From the equilibrium equation for the torques, it is found (Melton, 1970):

$$T = Sa^2 \sin \alpha - Sal_o \cos \frac{\alpha}{2} - Mg\, d \sin(\alpha+\delta) + h(\alpha - \alpha_o) \qquad (2.1)$$

where:

S = Spring rate (spring constant)

M = Inertial mass of the moving part

h = Hinge rate

l_o = Initial length of the spring

d = Distance from hinge to center of mass of the moving part

λ = Distance from hinge to seismometer scale

a = Distance from hinge to point of suspension of the spring

The La Coste seismometers use a spring with $l_o = 0$ i.e., the physical contraction of the spring to "zero length" corresponding to zero tension is prevented only by the interference of the coils with one another. If it is further assumed that the hinge rate is negligible, equation (1.2) becomes, at equilibrium:

$$T = Sa^2 \sin \alpha_o - Mgd \sin(\alpha_o+\delta) = 0 \qquad (2.2)$$

Although this equation can be satisfied in an infinite number of ways by varying the parameters, α_o, M and δ, the only way it can be satisfied at $\delta = 0$ is by setting the mass equal to:

$$M_{\delta=0} = m = \frac{Sa^2}{gd} \qquad (2.3)$$

The advantage of this design in the La Coste seismometer is that, at zero tilt, there is equilibrium at all positions, i.e., the natural period is infinite. With small departures in m or δ from that equilibrium state, equation (2.2) will be satisfied at only one α_o.

For both the Sprengnether and Geotech seismometers $\alpha_o = \pi/2$.

In this case, Equation (2.2) reduces to:

$$M = \frac{m}{\cos \delta} \tag{2.4}$$

Thus, when tilting the seismometer by δ, the mass has to be increased from m to M to keep α_o at 90°. The change in mass, or more precisely the change in the effective md product, is accomplished by sliding a small weight along the boom of the seismometer.

In angular harmonic motion, the period P is given by

$$P = 2\pi\sqrt{\frac{K}{U}} \tag{2.5}$$

where: K = Moment of inertia of the moving part

U = Change in torque per radian (torsional constant)

For small displacements from the equilibrium position:

$$U = \left.\frac{\partial T}{\partial \alpha}\right|_{\alpha=\alpha_o} \tag{2.6}$$

From (2.2):

$$U = Mgd \sin \delta \tag{2.7}$$

The moment of inertia can be written as:

$$K = M\rho^2 \tag{2.8}$$

where ρ= Radius of gyration.

Whence the equation for the period reduces to:

$$P = 2\pi\rho\sqrt{\frac{1}{gd \sin \delta}} \tag{2.9}$$

The natural period decreases for an increase in δ. With $1_o = 0$, only positive δ are considered as negative δ would give a resultant

torque in the same direction as the displacement in (2.2) and hence is unstable.

The geometry described here is that of the Sprengnether but in the case of the Geotech, the same principles apply. Although the geometry is changed, the relation $M = m/\cos\delta$ again results by setting the coefficients of $\sin\alpha_o$ and $\sin(\alpha_o + \delta)$ equal at zero tilt.

In the real instruments the springs have negative initial length, which means that the tension is so great that the two terminals, when released, would pass each other if possible. The zero length is obtained by use of a stiff link whose variable length is set equivalent to the negative length of the spring (Fig. 2).

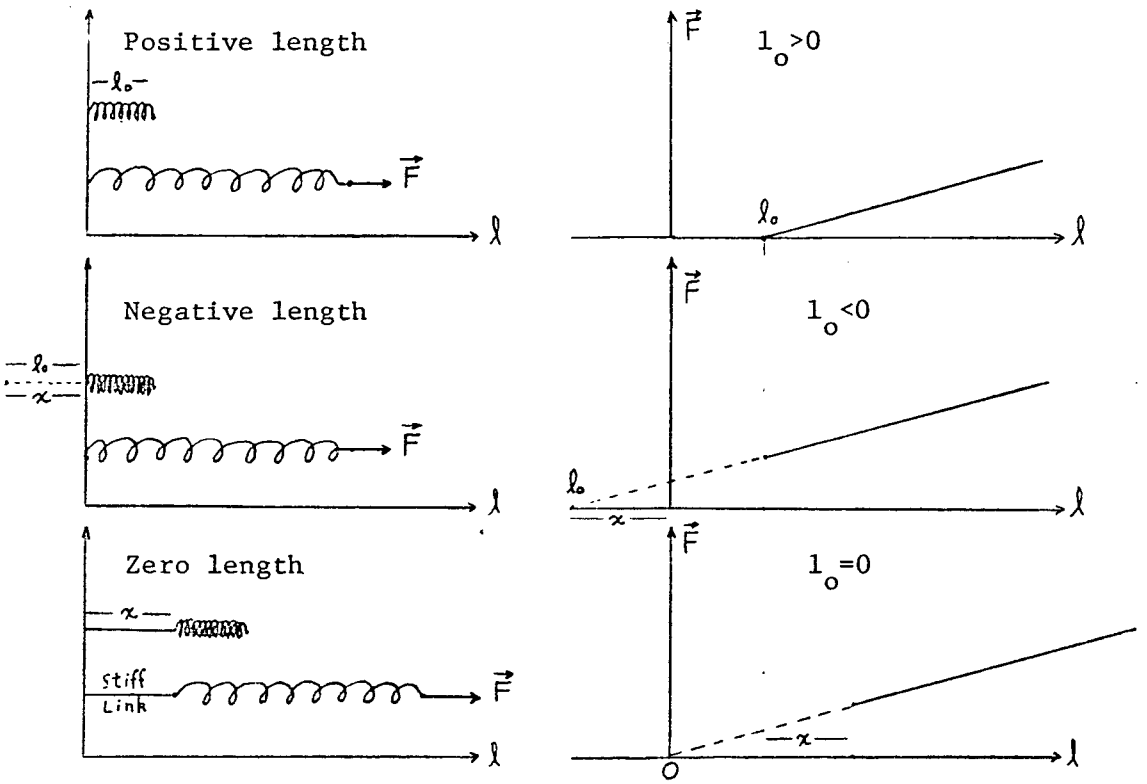

Fig. 2 Diagrammatic representations of the positive, negative and zero length springs and their force-extension relations.

2.2 Adjustment Procedures

Although manuals are provided with the seismometers, a more detailed description is given here in terms of the equations developed in the previous section in order that future workers may benefit from the author's experience.

It is suggested that the instruments be assembled according to the manufacturer's instructions with one exception. For the Sprengnether, it is preferable to postpone the mounting of the magnet to the end of the adjustment procedures since a small drag, probably of magnetic origin, hampers the free motion of the coil inside the magnet. This makes the measurement of the natural period difficult at small amplitudes since a sufficient number of free oscillations is necessary to obtain an average value for it.

After the seismometers have been leveled in both horizontal directions and the length of the stiff link adjusted so that the mass seems to be "about" to float at any position, they should in theory be close to the state represented by equation (2.2) with $\delta=0$. In practice, the infinite period condition is not attainable and after a certain time, the mass will start to drift to one of the stop positions. This is because $l_o \neq 0$ and therefore the term $- Sal_o \cos \frac{\alpha}{2}$ in (2.1) must be retained and/or (2.3) does not hold. One effect is indistinguishable from the other at this stage.

In the next operation, the seismometer is given a small positive tilt (about two turns of the single levelling screw) and

the natural period measured by giving a small impulse to the mass and feeding the signal to an oscilloscope. If the natural period is too far from the desired period (say more than two seconds), the tilt is changed in the direction given by equation (2.9). If the mass cannot be centered by sliding the small weight, the length of the stiff link is corrected accordingly.

At this point, equilibrium is reached as in equation (2.1) with T = 0 rather than as in (2.2). The zero length condition is not exactly satisfied however and this is very important because the period versus position curve will be symmetrical and flat relative to $\alpha_o = 90°$ only under the zero length condition (Melton, 1970). Therefore, the next step is to slide the small weight in order that the mass floats in both high and low positions relative to the scale center and to measure the period. If the period is longer when the mass is floating high, l_o is smaller than zero and vice-versa. The stiff link is lengthened if $l_o<0$ and shortened if $l_o>0$ and the mass readjusted. This step is very critical and after some trials, only extremely small changes are required to get a flat response. The center period might change slightly because of the variation in M; and the tilt has to be corrected once again. This should finally reduce the equilibrium equation to (2.2) with the value of M (or δ) that gives the proper period.

It is not an easy task to optimize the adjustment of the instruments because when one parameter is changed, it alters all the others. It is emphasized that one should consider each step in terms

of the effects on equations (2.1) and (2.2). More detailed consideration of these equations and worked out examples will be found in Melton (1970). Fig. 3 shows the actual period vs position curves obtained from the Sprengnether and the Geotech before proceeding to the other measurements. It is likely that additional adjustment on the Sprengnether would yield smaller deviations from the zero position value of period. However, variations in phase response as a function of mass position was found to be smaller than that of the Geotech for which the period changes less with position. The phase is also affected by the change in seismometer constants (Table I). It should be noted that the Geotech curve has a larger deviation than that shown in their manual. F. Kollar (private communication) also reports that the instruments of the Earth Physics Branch do not meet the manufacturer's specifications.

2.3 Temperature Effects

An important cause of variations in α_o is thermal instability. To find the effects of temperature fluctuations on the mass position, the seismometers were covered by a styrofoam case containing electric light bulbs as a heat source. The temperature was regulated by a thermostat and measured with a differential thermocouple. Fig. 4 shows the mass position vs temperature curves for the Sprengnether and the Geotech. The Sprengnether spring has a positive coefficient of thermal expansion while that of the Geotech is negative. It is noted that the mass position as a function of temperature is approximately linear with deviations from the straight line normally being less than 1 mm.

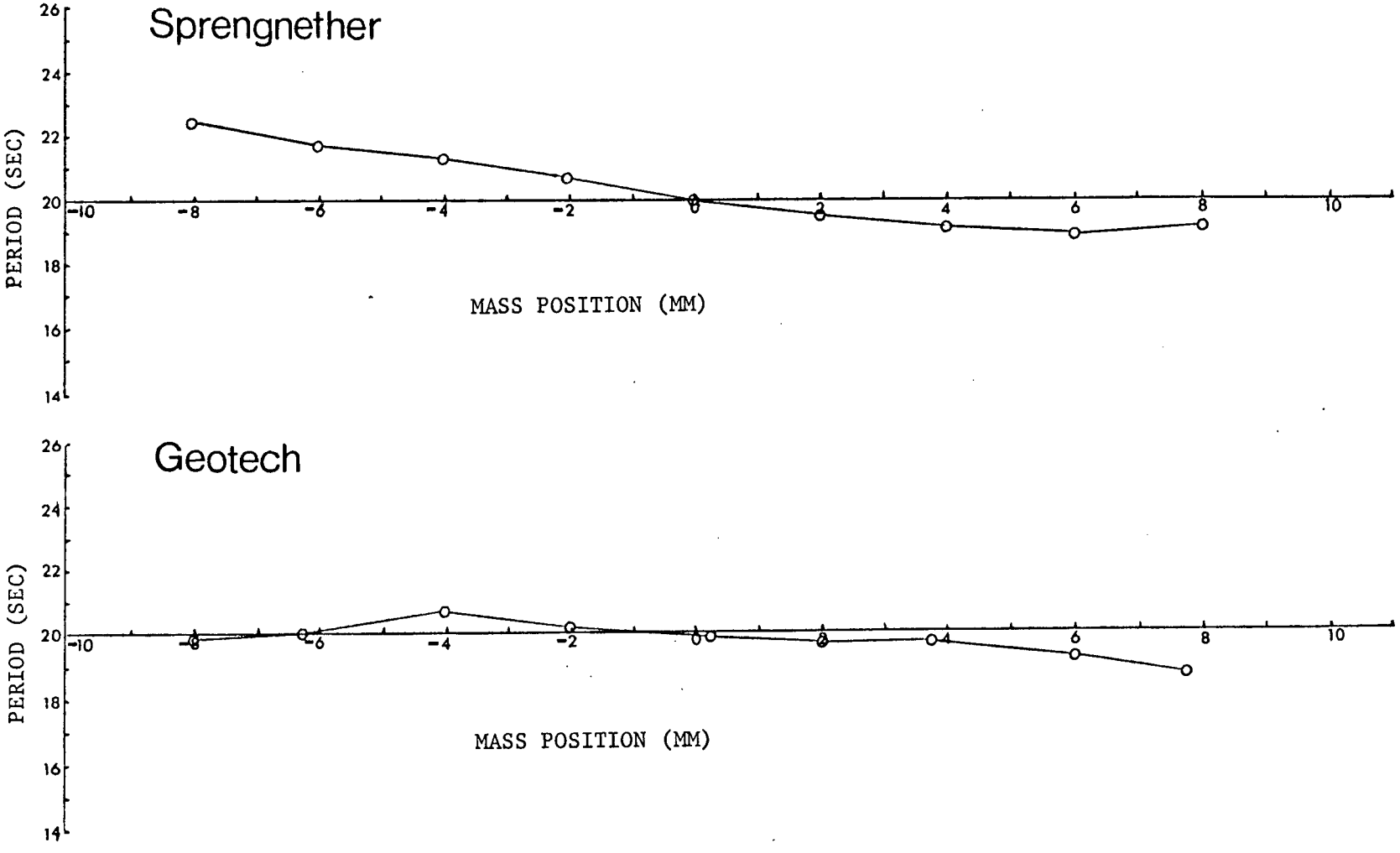

Fig. 3 Period vs. mass position for the Sprengnether and Geotech seismometers.

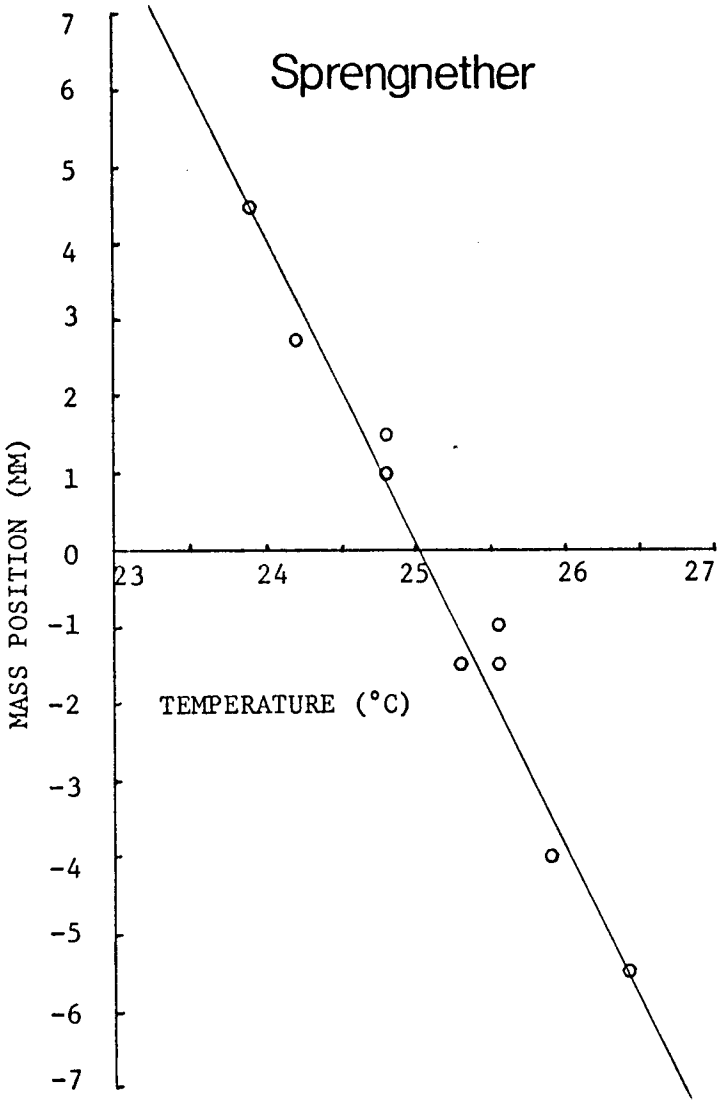

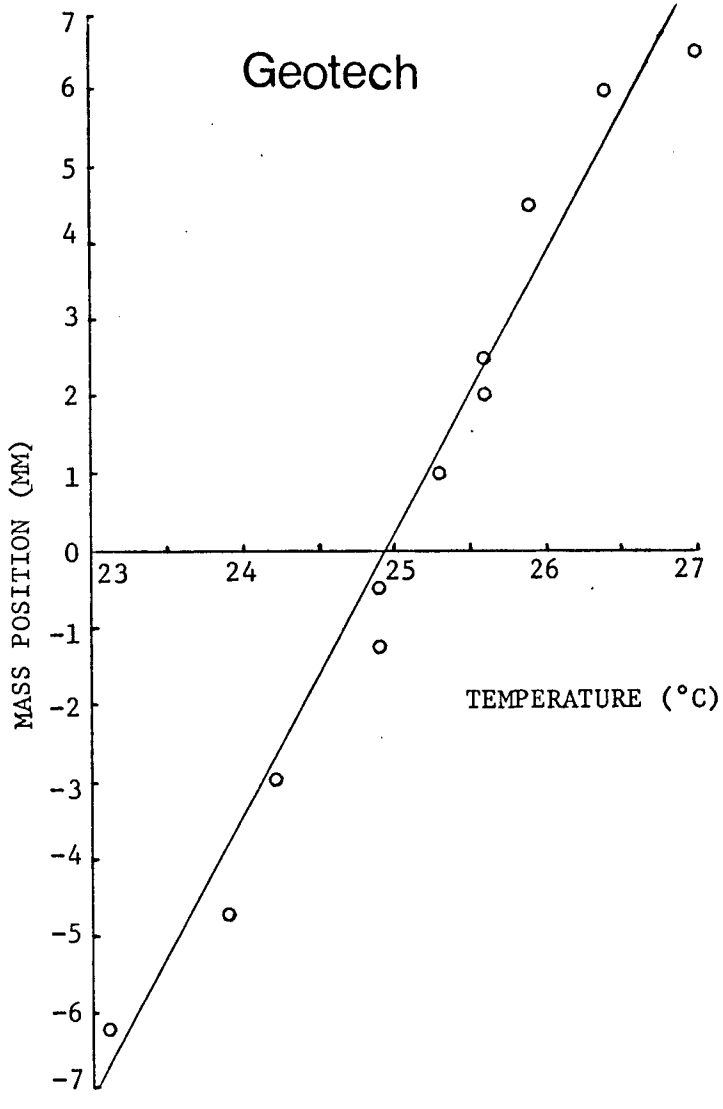

Fig. 4 Mass position vs. temperature for the Sprengnether and Geotech seismometers.

In an operational system an additional complication arises due to drift in the temperature controllers themselves. Over a short period (1 week), this drift may lead to a change in mass position of ±3 mm. Over an interval of a month drifts as large as ±6 mm were observed. As this corresponds to significant changes in phase response, the system should be checked at frequent intervals. Further effort might also be expended in controller design.

2.4 Pressure Effects

In the equilibrium equation for the torques (2.1), it was assumed that the density of the air ρ_o was a constant. Since a pressure change dP_o may change ρ_o, it was necessary to find the effect of such a change on the zero stability of the seismometer. With ρ, the density of the mass, equation (2.1) is now written as:

$$T = Sa^2 \sin\alpha - Sal_o \cos\frac{\alpha}{2} - Mgd\left(1 - \frac{\rho_o}{\rho}\right)\sin(\alpha + \delta) + h(\alpha - \alpha_o) \qquad (2.10)$$

With ρ_o and α as variables:

$$dT = \frac{\partial T}{\partial \rho_o} d\rho_o + \frac{\partial T}{\partial \alpha} d\alpha \qquad (2.11)$$

At equilibrium (dT=0):

$$d\alpha = \left[\frac{-\frac{\partial T}{\partial \rho_o}\Big|_{\alpha=\alpha_o}}{\frac{\partial T}{\partial \alpha}\Big|_{\alpha=\alpha_o}} \right] d\rho_o \qquad (2.12)$$

From (2.6):

$$d\alpha = -\frac{1}{U}\left[\frac{\partial T}{\partial \rho_o}\Big|_{\alpha=\alpha_o}\right] d\rho_o \qquad (2.13)$$

From (2.10):

$$d\alpha = - \frac{Mgd}{U\rho} \sin (\alpha_o + \delta) \, d\rho_o \tag{2.14}$$

Assuming isothermal pressure changes:

$$\frac{\rho_o'}{\rho_o} = \frac{P_o'}{P_o} \tag{2.15}$$

$$d\rho_o = \frac{\rho_o}{P_o} \, dP_o \tag{2.16}$$

Furthermore:

$$d\alpha = - \frac{dx}{\lambda} \tag{2.17}$$

From (2.14), (2.16) and (2.17) at $\alpha_o = 90°$:

$$dx = \frac{Mgd\lambda\rho_o \cos\delta}{U\rho P_o} \, dP_o \tag{2.18}$$

For example, for the Sprengnether:

$M = 11.2$ kg

$g = 9.8$ m/s^2

$d = .308$ m

$\lambda = .454$ m

$\delta = 3°$

$U = .121$ kg m^2/s^2

$\rho_o = 1.293$ kg/m^3

$\rho_{lead} = 11300$ kg/m^3

For a large pressure change of 2 cm at a normal pressure of 76 cm:

$$dx = .4 \text{ mm} \tag{2.19}$$

With a drift of the same order for the Geotech, it is concluded that pressure changes of this magnitude cannot affect the zero stability significantly. However, it is still very important to have the seismometer tightly sealed since a rapid change in pressure
be equivalent to a strong signal from the ground.

2.5 The Seismometer Constants

As the general theory for seismometer calibration can be found in Russell and Kollar (1966), a detailed development will not be given here. Their equations for a "mass on a spring" seismometer have been modified to suit the pendulum seismometer. Consider Fig. 1 with an initial frame of reference y (positive downward) relative to the surface of the Earth and the pendulum hinge at the origin O of an x, ϕ system moving with the seismometer case. A coil of impedance Z_c fixed to the boom swings through a magnet and produces a current I through a load Z_L. The following symbols are adopted:

ϕ: Displacement from equilibrium position: $\phi = \alpha - \alpha_o$

D: Damping moment constant (kg m^2/s)

U: Spring moment constant (kg m^2/s^2):

G: Coil motor constant (kg m^2/As^2)

l_c: Distance from hinge to center of gravity of the moving part

l_p: Distance from hinge to center of oscillation (reduced pendulum length)

T_N: Natural period

For small displacements the equations of motion are:

$$K\ddot{\phi} + D\dot{\phi} + U\phi = Ml_c\ddot{y} - GI \tag{2.20}$$

$$G\dot{\phi} = (Z_c + Z_L)\, I \tag{2.21}$$

The load includes the attenuating resistors, the input impedance of the amplifier and the filters if any. These two equations are completely equivalent to the nodal and loop equations of the circuit of Fig. 5.

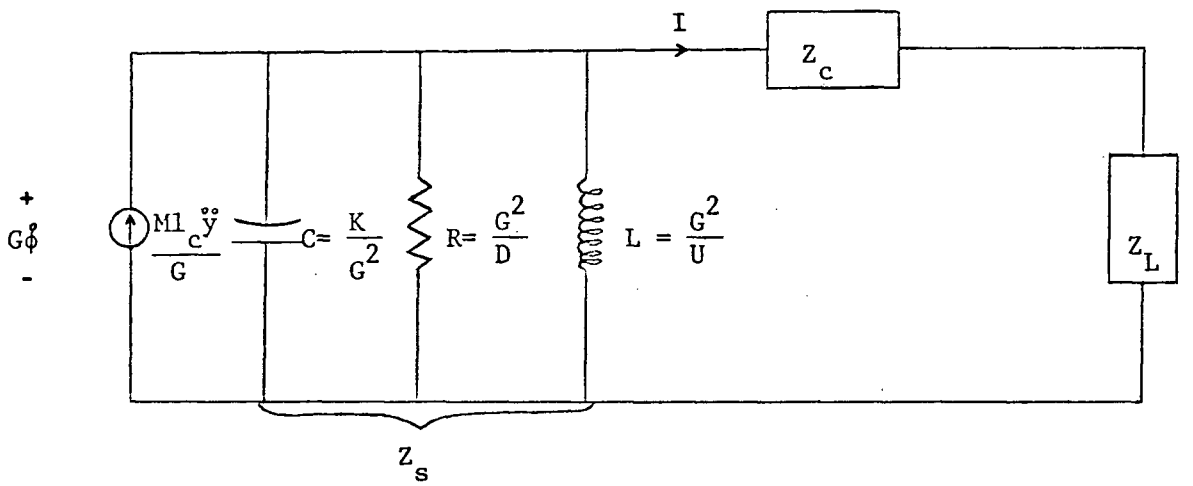

Fig. 5 The equivalent electrical circuit for the seismograph.

Since the electromechanical seismometer is indistinguishable from its purely electrical equivalent, the above circuit will be used in the analysis.

For calibration purposes the seismometer is placed in the Maxwell bridge (Fig.6). To find Z_c, the seismometer is clamped and the bridge is balanced. Then Z_c is given by:

$$Z_c = R_B R_R / Z_B \qquad (2.22)$$

The locking mechanism of the Sprengnether is not tight enough to avoid the mass moving slightly under balance condition and an additional heavy weight must be placed on the mass to make it completely immovable and prevent a false balance condition. For both seismometers, the balance condition is found to be frequency dependent. The effects of

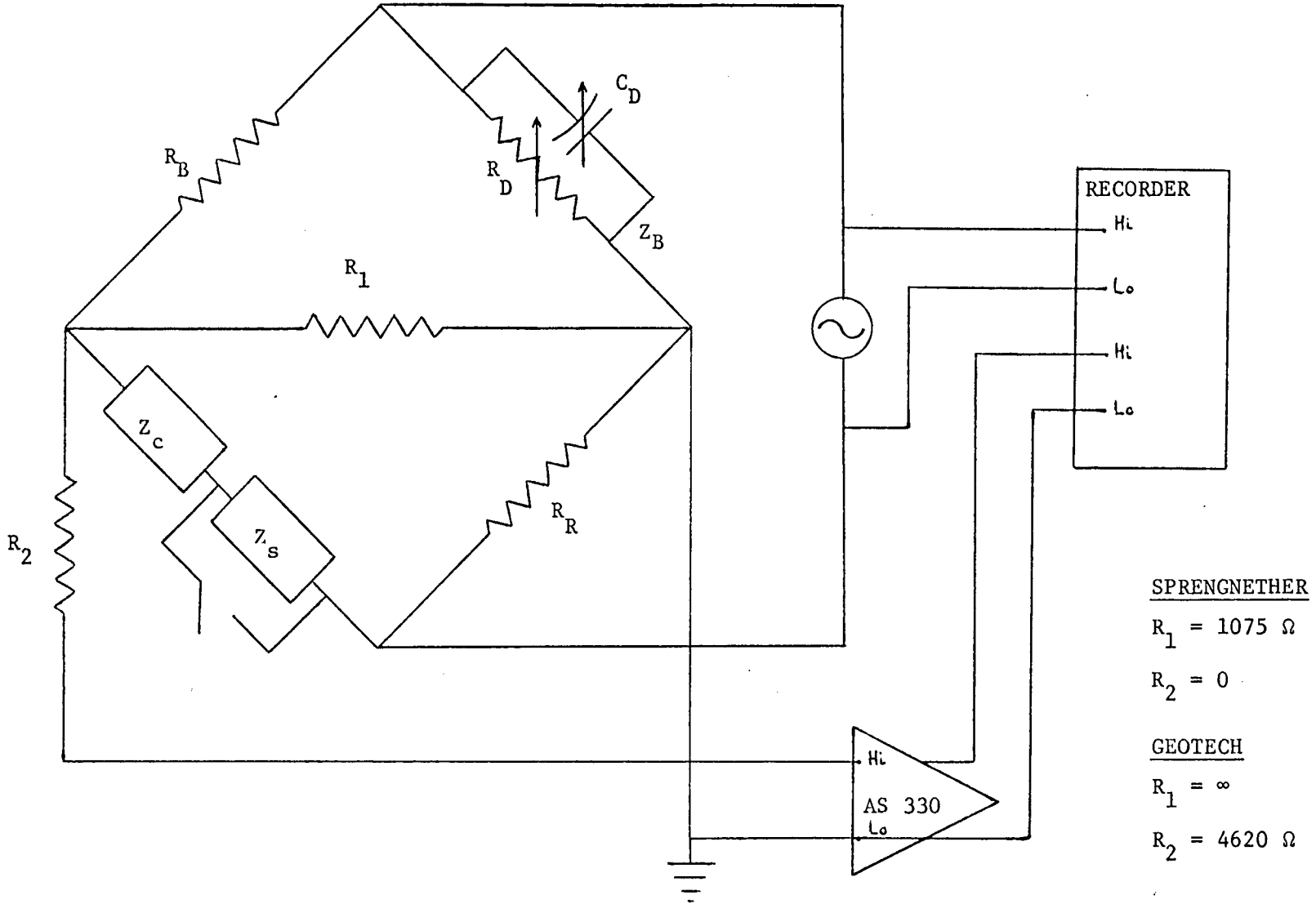

Fig. 6 The Maxwell bridge calibration system with the AS-330 amplifier and chart recorder as the detection device.

hysteresis and eddy current losses must be taken into consideration. Those effects are observed at frequencies much higher than that for which the seismometers are designed to operate. However, we shall see that the amplitude response must be determined over a wide frequency range if the phase response is to be determined directly from it.

At low frequencies the coil of the seismometer is adequately represented by a series connection of a resistance r and an inductance l. At higher frequencies, Shima (1959) uses a loss resistance q in parallel with the inductance as in Fig. 7(a). This is easily transformed in the form of Fig. 7(b) by:

$$r' = \frac{q}{\left[1 + \left(\frac{q}{\omega l}\right)^2\right]} \tag{2.23}$$

$$l' = \frac{l}{\left[1 + \left(\frac{\omega l}{q}\right)^2\right]} \tag{2.24}$$

$$Z = r + r' + l' \tag{2.25}$$

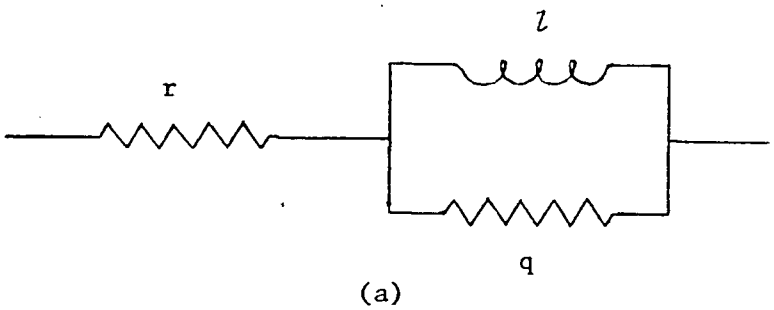

(a)

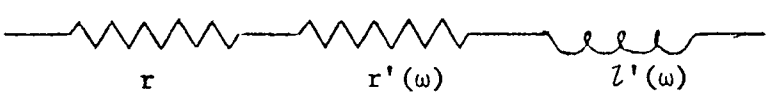

(b)

Fig. 7 Equivalent circuit of the coil of seismometer

Formulas (2.23) and (2.24) show that the resistance r + r' seen by the bridge should increase with frequency and the inductance l' should decrease. This is observed experimentally (Fig. 8) although no single loss resistance that would fit both curves simultaneously could be found. Clearly the model of Shima is only an approximation.

The Willmore method is used to find the other constants. The seismometer is unclamped and a series of output voltages from the main (V_M) and substitution (V_S) inputs are recorded. Russell and Kollar (1966) point out that V_M/V_S is completely independent of Z_L and is given by:

$$\frac{V_M}{V_S} = \frac{R_E}{R_R R_B} Z_s \tag{2.26}$$

From Fig. 5, it is seen that in terms of the complex frequency $s = \sigma + j\omega$:

$$Z_s = \frac{G^2 s}{Ks^2 + Ds + U} \tag{2.27}$$

The $|Z_s|$ curve for the center position of the Sprengnether and the Geotech are shown in Fig. 9 and Fig. 10.

All the constants were calculated and collected in Table I. The moment of inertia was found by the relation:

$$K = M l_c l_p \tag{2.28}$$

The other parameters were determined from the asymptotes and the maximum of the $|Z_s|$ curve and from the natural period of the seismometer. Those parameters are those that will be used in the next two chapters to find the amplitude and phase response of the seismometers at the +6mm, 0mm, -6mm equilibrium positions.

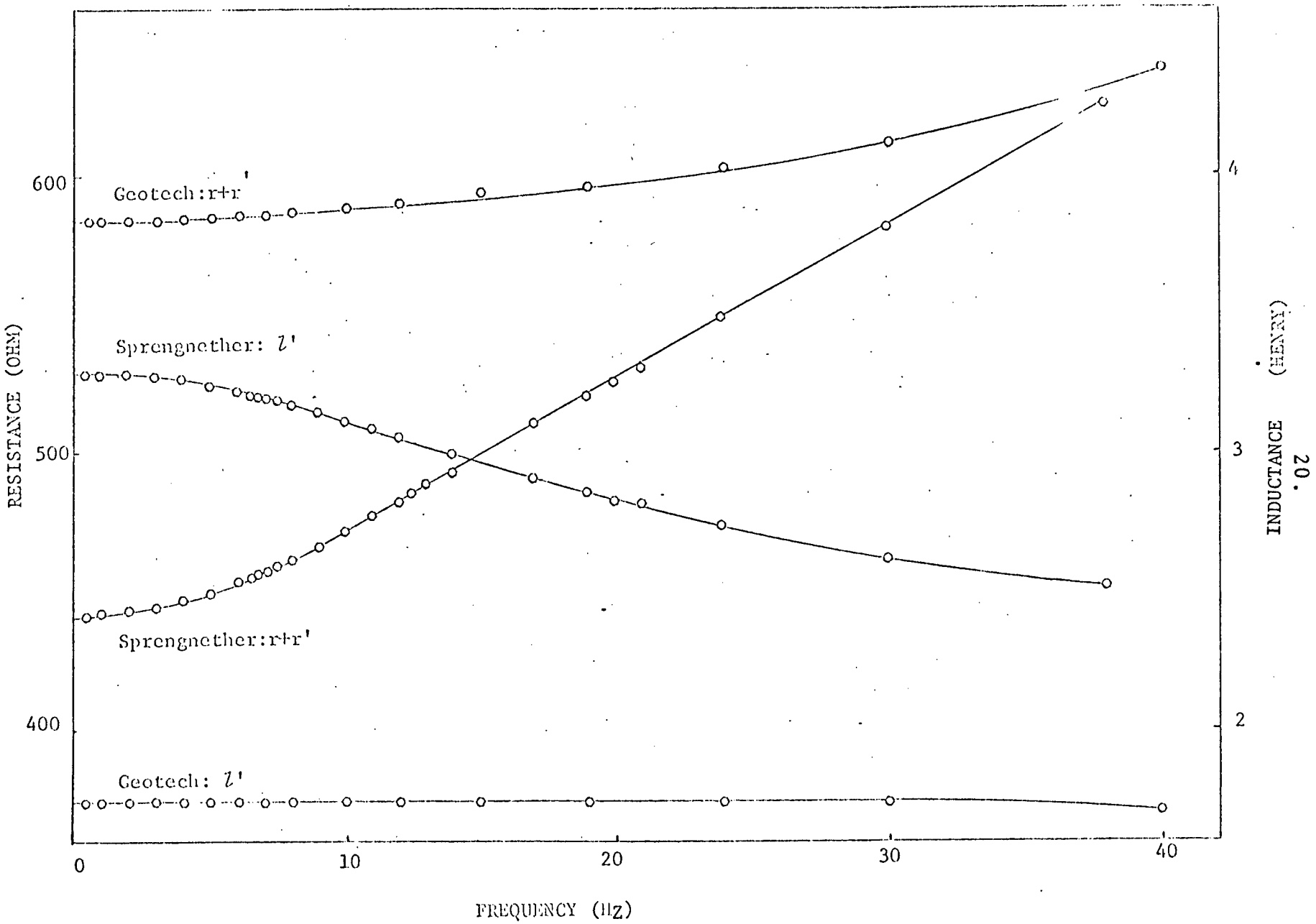

Fig. 8 Resistance and conductance of the coil of the Sprengnether and the Geotech at central position.

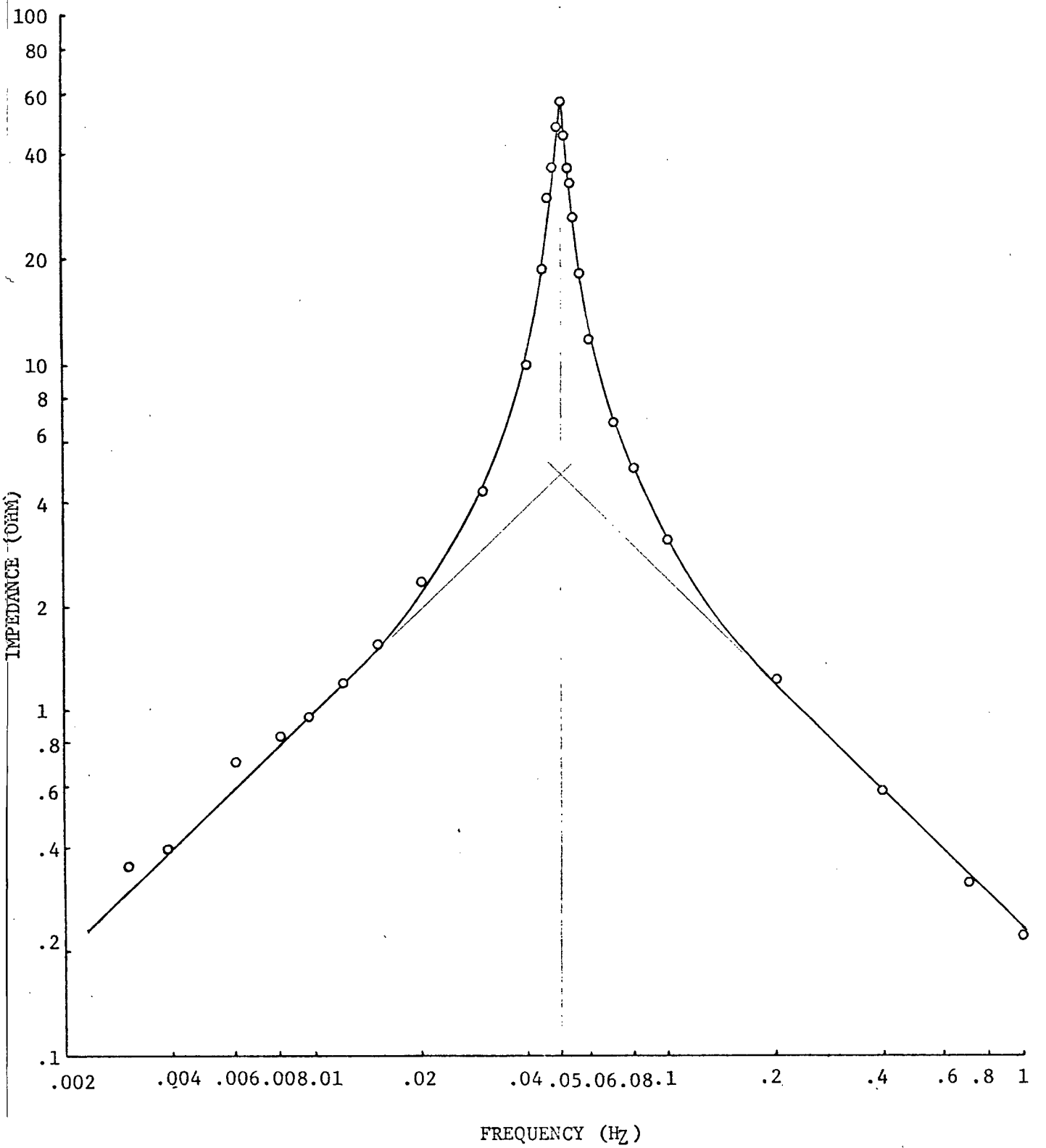

Fig. 9 Equivalent impedance of the Sprengnether seismometer

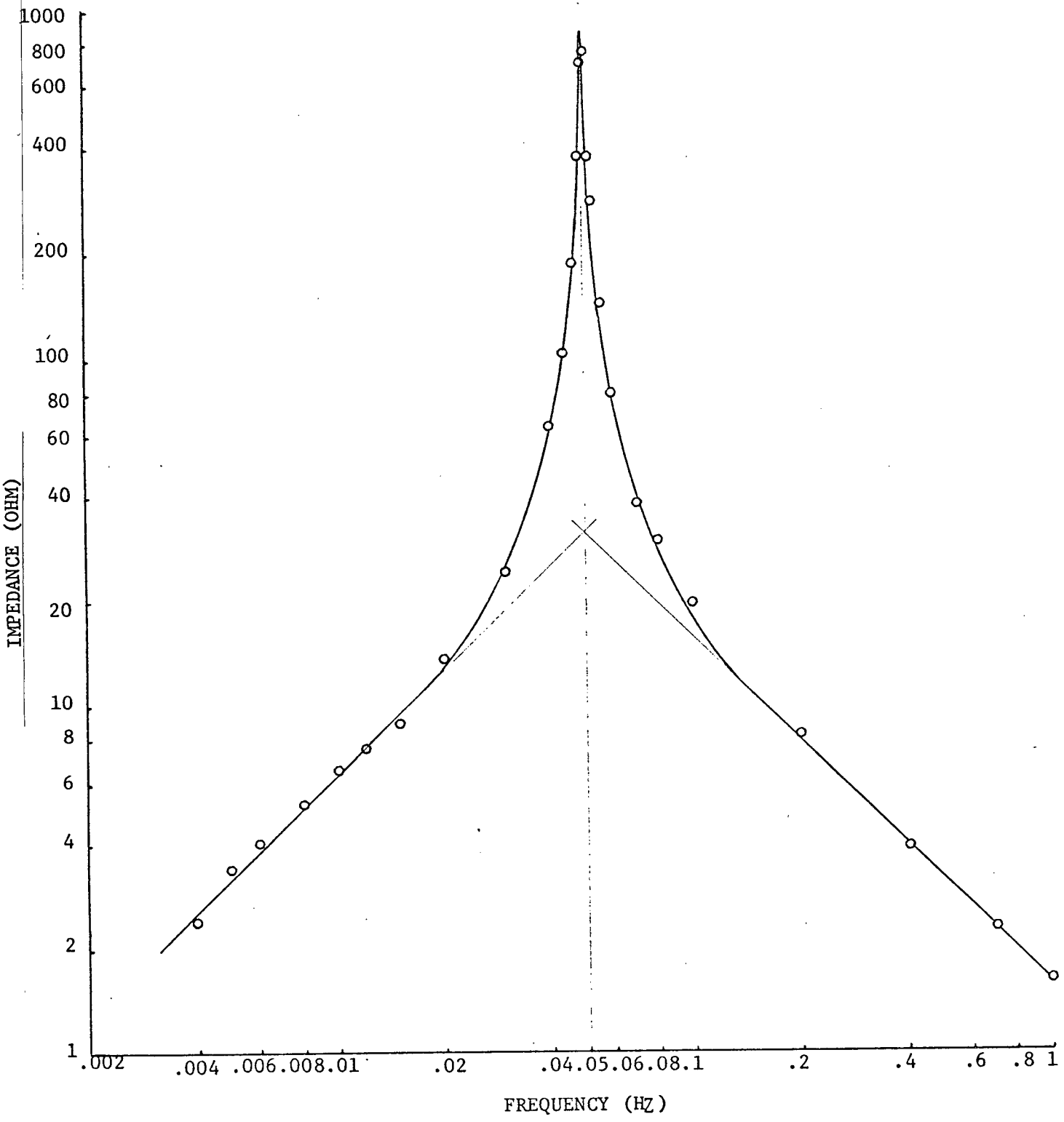

Fig. 10 Equivalent impedance of the Geotech seismometer

Seismometer	Position(mm)	Temperature (°C)	G(kgm^2/As^2)	D(kgm^2/s)	U(kgm^2/s^2)	T_N(sec)
Sprengnether:	+6	≃23.5	27.7	.0640	.131	19.2
l_p: .3564m	0	≃25.	27.7	.0318	.121	20.0
K = 1.23 kgm^2	-6	≃26.5	27.7	.0248	.098	22.2
Geotech	-6	≃23.5	21.5	.00220	.0114	20.4
l_p = .30m	0	≃25.	22.4	.00142	.0121	19.8
K = .12 kgm^2	+6	≃26.5	20.9	.00406	.0128	19.2

Table I. Seismometer constants.

Chapter III

The Amplitude Response

3.1 The Response of the Seismometer

As well as being used to determine the seismometer constants, the Maxwell bridge can be used to find the amplitude response of the complete seismograph. With the bridge balanced at all frequencies and an appropriate choice of impedances in the circuit, the currents through R_B, C_D, and R_D and R_E may be neglected and the equivalent of the seismometer in the bridge may be reduced to a ladder circuit (Russell and Kollar, 1966). For analytical purposes, it is convenient to divide the seismograph into its three components (Fig. 11) and find the transfer functions of the seismometer F_S, of the amplifier F_A and the recorder F_R.

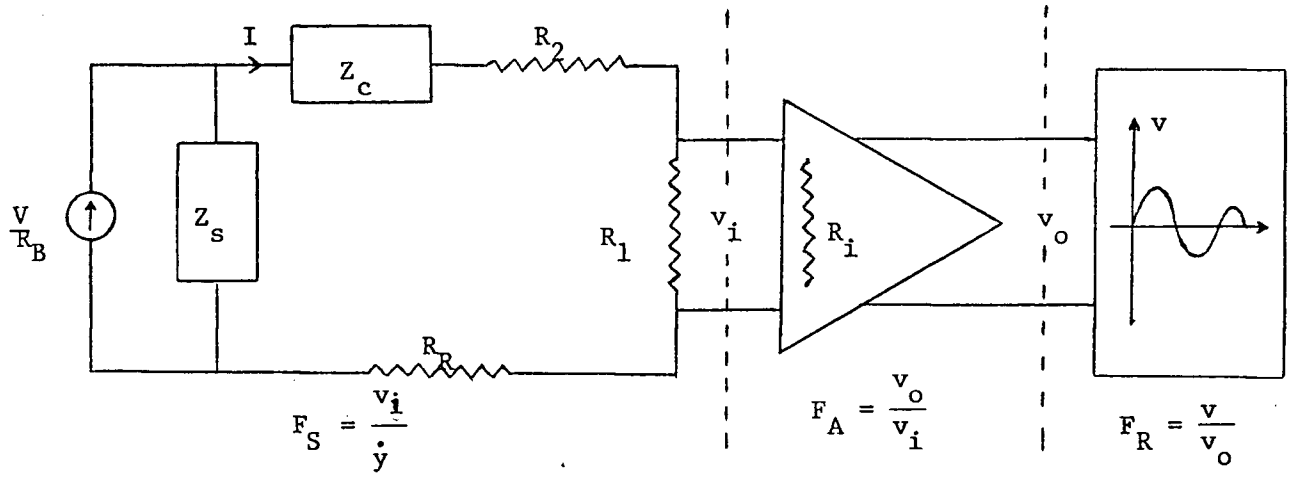

Fig. 11 Circuit of the balanced seismograph

For convenience we define an effective input impedance of the amplifier Z_i by

$$Z_i = \frac{R_1 R_i}{R_1 + R_i} \tag{3.1}$$

The damping resistance R_D is then given by:

$$R_D = r + r' + R_R + R_2 + Z_i \tag{3.2}$$

From the circuit of Fig. 11 the input voltage to the amplifier is readily found as:

$$v_i = \frac{VZ_iZ_s}{R_B(Z_s + s\ell' + R_D)} \tag{3.3}$$

and from Fig. 5, the source current is equivalent to:

$$\frac{V}{R_B} = \frac{Ml_c\ddot{y}}{G} \tag{3.4}$$

By integrating (3.4) and using (2.28), the equivalent ground velocity is found to be:

$$\dot{y} = \frac{Vl_pG}{R_BK_s} \tag{3.5}$$

By (2.27), (3.3) and (3.5), the transfer function $(v_i/\dot{y})$ of the seismometer is given by:

$$F_S = \frac{GKZ_is^2}{l_p[K\ell's^3 + (D\ell'+KR_D)\,s^2 + (G^2 + \ell'U + DR_D)s + R_DU]} \tag{3.6}$$

Since the ℓ' terms are small and decrease relatively with increasing frequency, they can be dropped and equation (3.6) reduces to:

$$F_S = \frac{GKZ_is^2}{l_p[KR_Ds^2 + (G^2 + DR_D)s + R_DU]} \tag{3.7}$$

At low frequencies:

$$F_{S_L} = \frac{GKZ_is^2}{l_pR_DU} \tag{3.8}$$

At high frequencies:

$$F_{S_H} = \frac{GZ_i}{l_p R_D} \tag{3.9}$$

On a Bode diagram, F_{S_L} will be a straight line of slope +2 and F_{S_H} a straight line of slope 0 as long as r' does not grow indefinitely. In Shima's model, its limiting value is that of the loss resistor. The corner is at the natural frequency of the seismomter:

$$\omega_S = \sqrt{\frac{U}{K}} \tag{3.10}$$

3.2 The Response of the Seismograph

In neither case was the complete transfer function (v_o/v_i) of the PTA and SSA amplifiers given by the manufacturer.

The transfer function of the PTA at maximum gain is given in Fig. 12; the slopes of the low and high frequency asymptotes are +3 and -4 respectively with corner frequencies $f_L = .0093$ and $f_H = 6.00$. The transfer function of the SSA is given in Fig. 13 at the maximum gain available from the low level output; in this case the low and high frequency asymptotes have slopes of +2 and -2 with corners at $f_L = .0094$ and $f_H = 4.77$. Finally, the transfer function of the recorder (v/v_o) will affect the amplitude response of the seismograph.

The total velocity response becomes:

$$F = \frac{v_i}{\dot{y}} \cdot \frac{v_o}{v_i} \cdot \frac{v}{v_o} \tag{3.11}$$

$$F = F_S F_A F_R \tag{3.12}$$

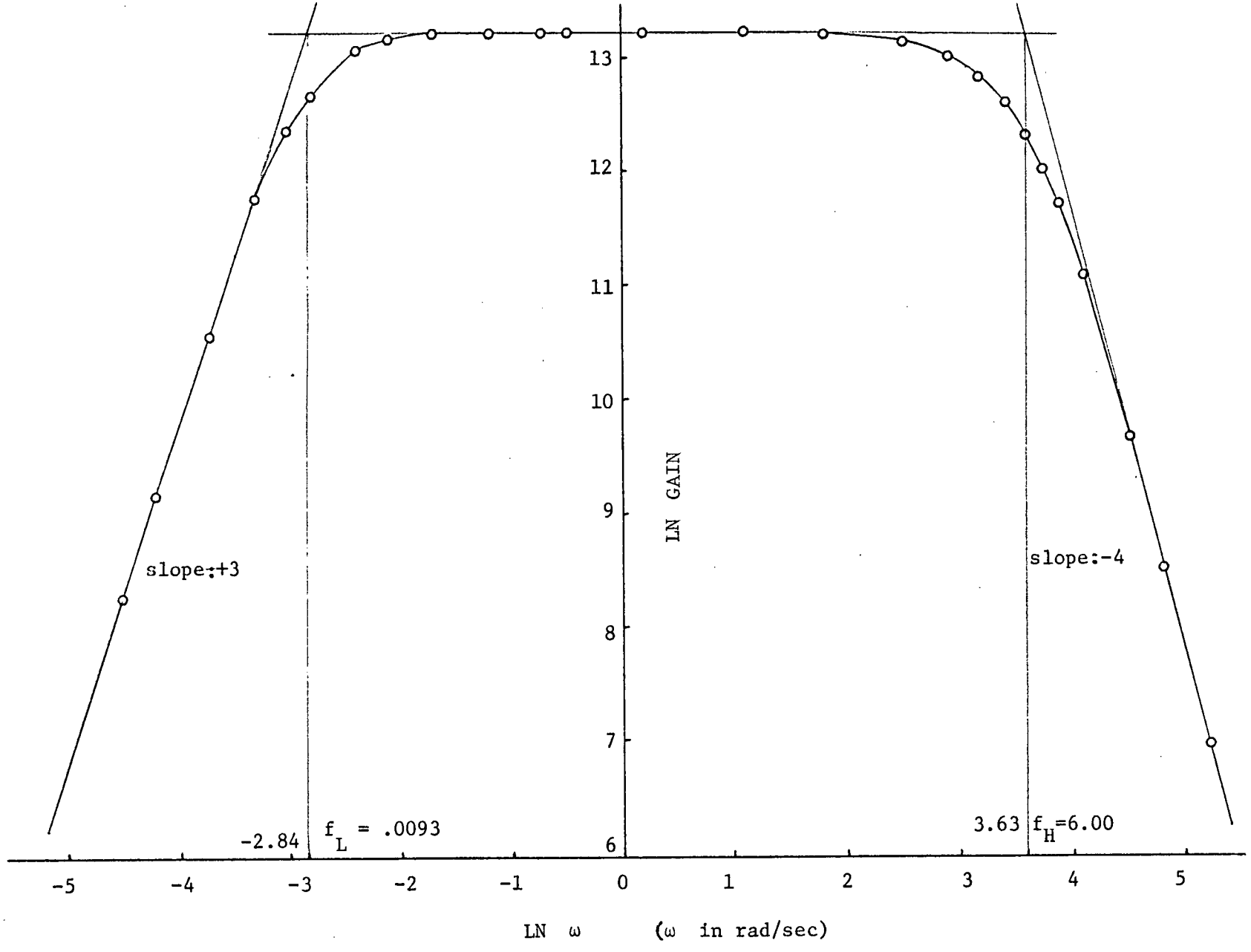

Fig. 12 Gain of the Geotech phototube amplifier (PTA)

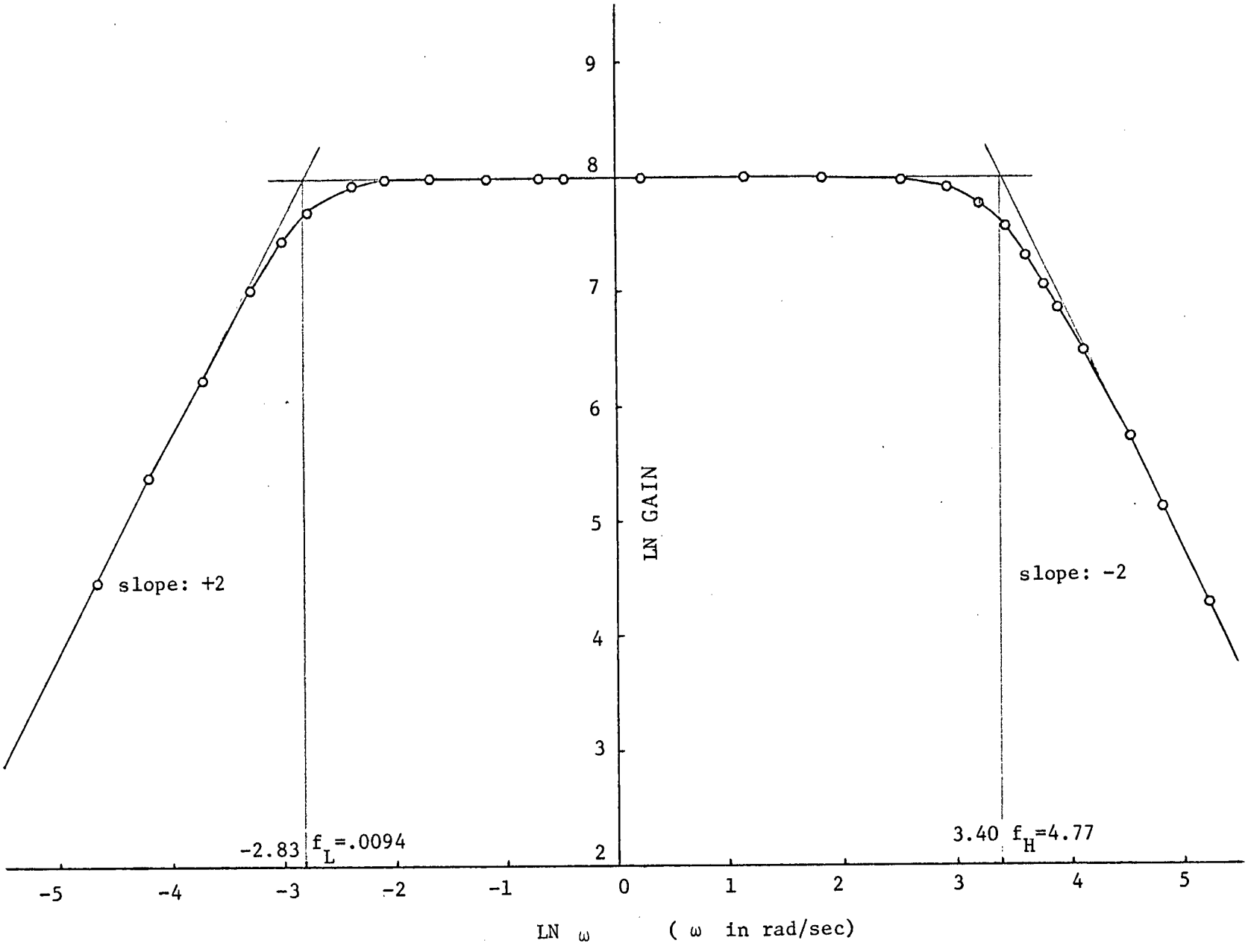

Fig 13: Gain of the Geotech solid state amplifier (SSA).

Or from (3.5):

$$F = \frac{v\, R_B Ks}{Vl_p G} \tag{3.13}$$

The coupling of the seismometer to the amplifier is taken into account through Z_L; it is assumed that the input impedance of the recorder is high and purely resistive. If not, or if there is a filter in between, the transfer function of the amplifier must be taken through the actual impedance of the recording stage. By (3.12) the asymptotic behaviour of the whole system is easily found on a Bode plot (Fig. 14). The slopes of each component are simply added between each corner. The acceleration, velocity and amplitude responses of the seismographs with the Sprengnether and the Geotech at center position are shown in Fig. 15 and Fig. 16. The amplifier used is the AS-330 and the recorder is the Brush 480 model 15-6687-00. The oscillatory behaviour of the Sprengnether curve at higher frequencies is attributed to resonances at the natural frequencies of its suspension spring. This was deduced from the fact that when the sliding weight was shifted to the right and the spring became tighter, the resonance peaks were shifted to higher frequencies and vice versa for a less tight spring. It was also observed that when the spring was tapped, beats were present in this frequency range.

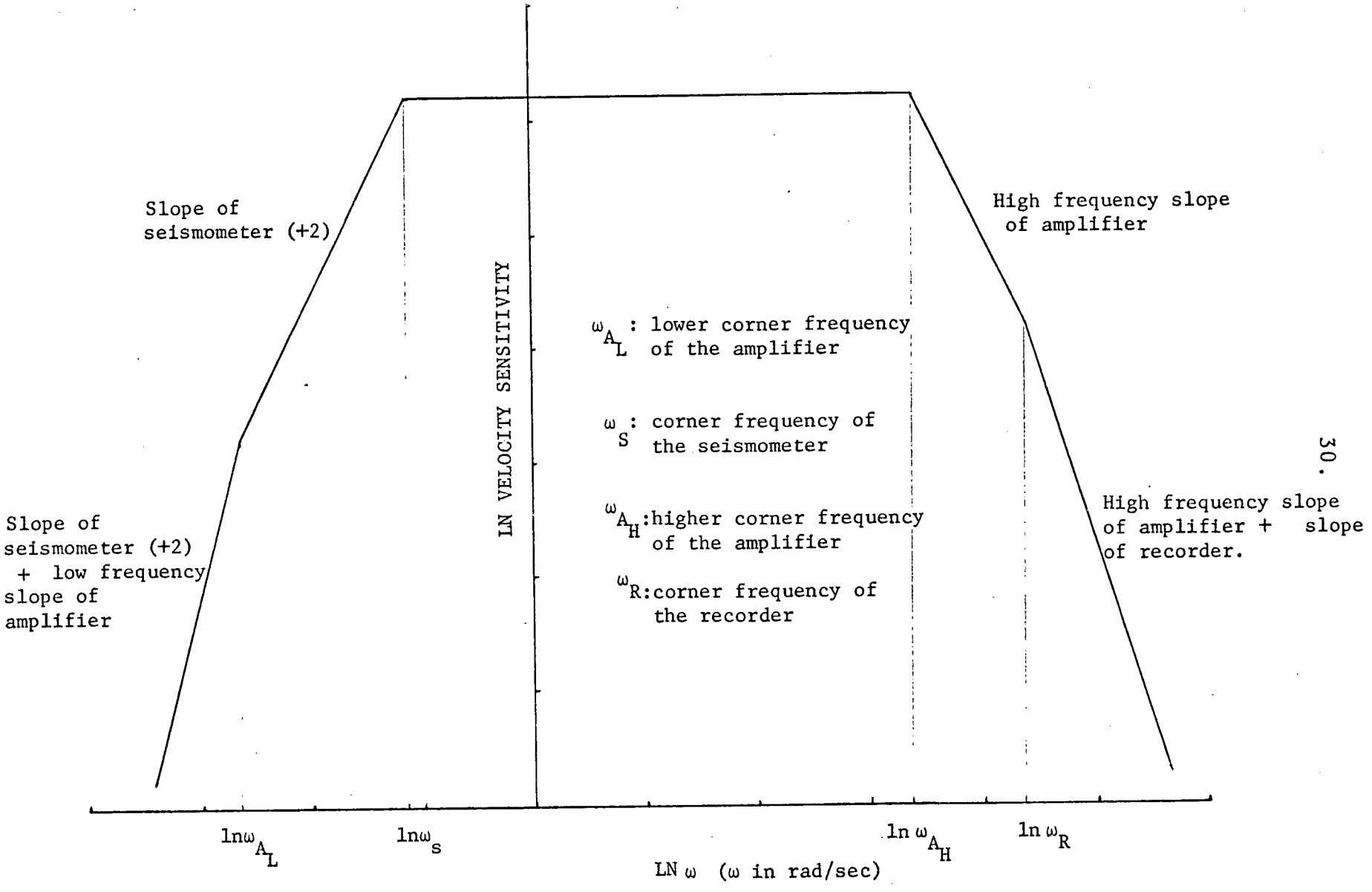

Fig. 14 Asymptotic behaviour of the velocity sensitivity curve of the electronic seismograph.

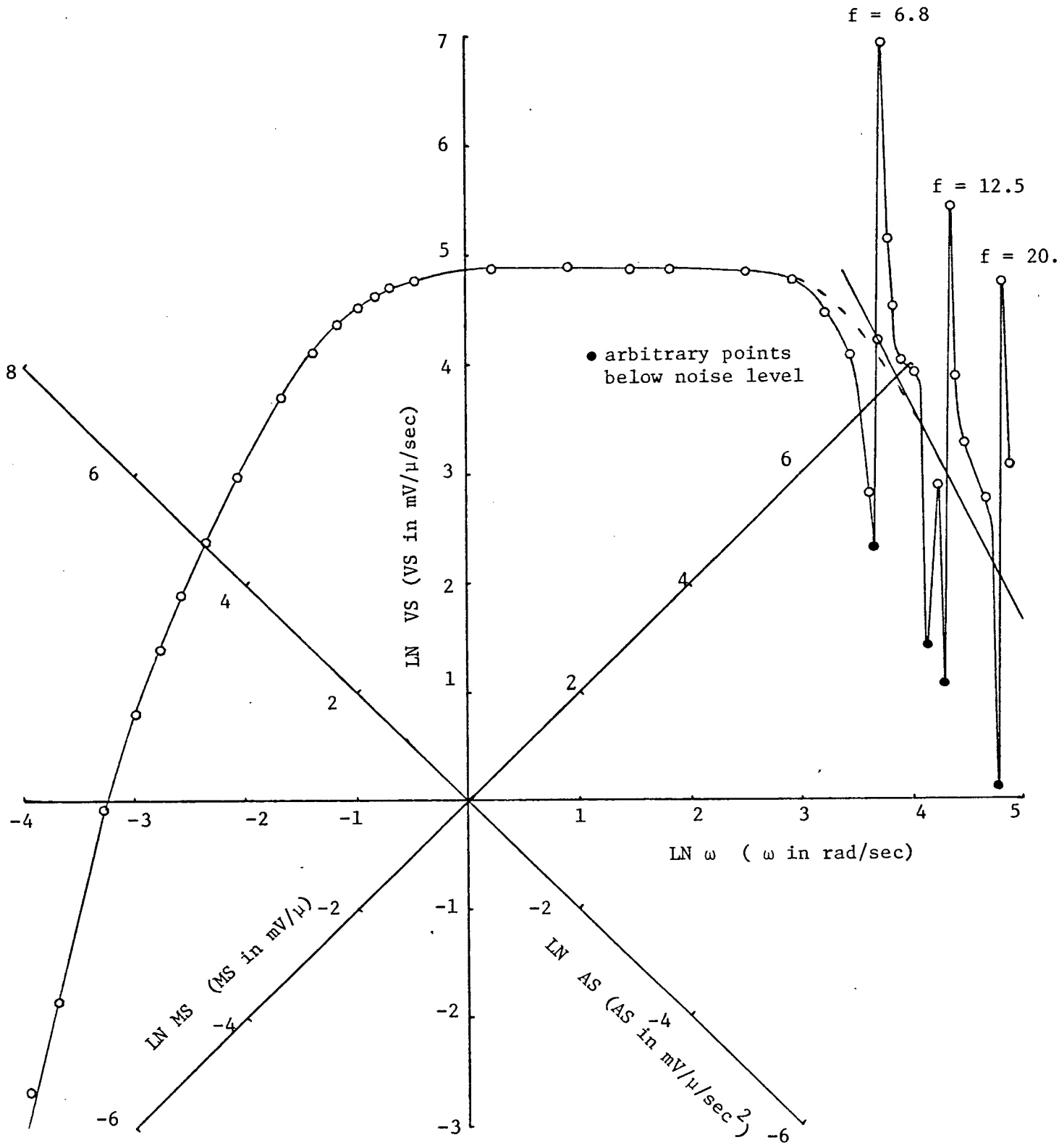

Fig. 15 Acceleration sensitivity (AS), velocity sensitivity (VS) and magnification (MS) of the Geotech seismometer-solid state amplifier(SSA) combination at center position.

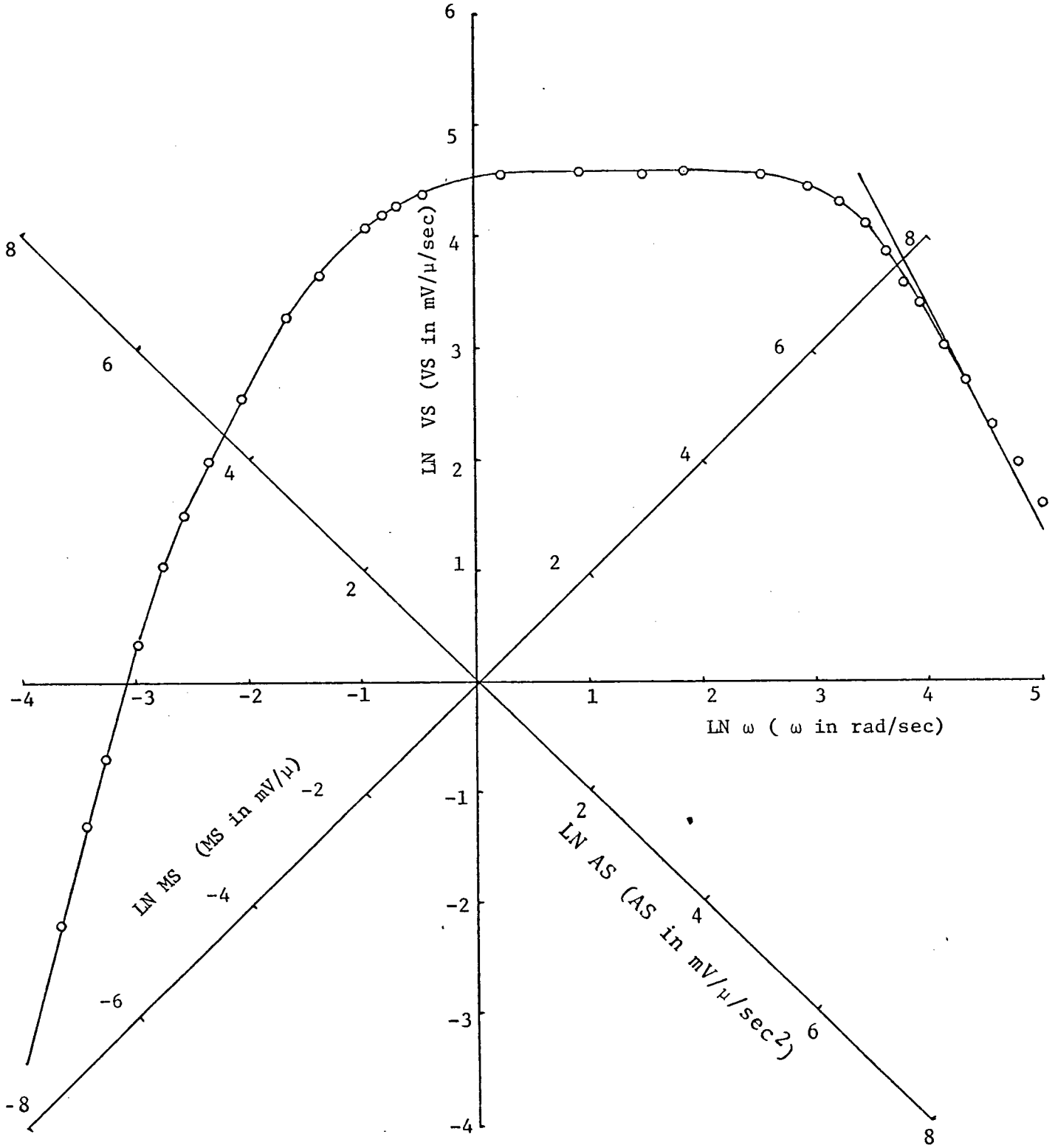

Fig. 16 Acceleration sensitivity (AS), velocity sensitivity(VS) and magnification (MS) of the Geotech seismometer-solid state amplifier (SSA) combination at center position.

Chapter IV

The Phase Response

4.1 Introduction

The direct procedure for obtaining the phase response of the seismograph is to measure the phase difference between the voltage applied to the bridge and the output voltage from the seismograph. However, the phase response may also be obtained from the amplitude response without additional measurements. In the following sections this procedure will be investigated in some detail.

4.2 Amplitude-Phase Relations

In this section several basic ideas of linear systems theory are outlined. For a more detailed exposition the reader is referred to Papoulis (1962).

In general, for a causal system a unique relation between the amplitude and phase of the transfer function F(s) does not exist. For a stable system, F(s) contains no poles in the right half plane or on the ω-axis. In this case $s = j\omega$ and the response in terms of the amplitude $H(\omega)$ and phase $\Phi(\omega)$ can be written

$$F(j\omega) = A(\omega)\, e^{j\Phi(\omega)} \tag{4.1}$$

Taking the logarithm of both sides yields:

$$\ln F(j\omega) = \ln A(\omega) + j\Phi(\omega) \tag{4.2}$$

For a complex function of s, a unique relation exists between the real and imaginary parts provided it has no singularities in the right half-plane. That is, $\Phi(\omega)$ may be found directly from $A(\omega)$ (and vice versa) provided that lnF(s) has no singularities in the right half-plane. For this to hold an additional condition on F(s) is required;

namely, F(s) has no zeros for Re s>0. The relationships between $A(\omega)$ and $\Phi(\omega)$ known as Hilbert transforms are:

$$\ln A(\omega) = -\frac{1}{\pi}\int_{-\infty}^{+\infty} \frac{\Phi(u)}{u-\omega}\, du \qquad (4.3)$$

$$\Phi(\omega) = \frac{1}{\pi}\int_{-\infty}^{+\infty} \frac{\ln A(u)}{u-\omega}\, du \qquad (4.4)$$

Henceforth, the frequency for which the phase is calculated is designated ω and the frequency of the recorded amplitude is designated u. Further, we define $L(u) = \ln A(u)$.

4.3 Minimum-Phase

Functions of the type described above are called "minimum-phase". The reason for this will become clear with the following argument. Consider a transfer function which has a zero in the right half plane:

$$T(s) = \frac{N(s)\ (1-as)}{D(s)} \quad (a>0) \qquad (4.5)$$

This can be rewritten as:

$$T(s) = \left[\frac{N(s)\ (1+as)}{D(s)}\right] \cdot \left[\frac{(1-as)}{(1+as)}\right] \qquad (4.6)$$

T(s) is the product of two complex functions, but the second term is a pure phase shifter, that is its modulus is always equal to unity and its phase varies from 0 to $-\pi$. This means that given a function with a zero in the right half plane, one can always find another function with the same gain but with a smaller lag. In the illustration $N(s)\ (1+as)/D(s)$ is the minimum phase function with the same amplitude as T(s). Since there are no zeros in the right half plane, a pure phase shifter cannot be extracted which decreases the phase.

The transfer function of the seismograph is minimum phase since

the amplifier and the recorder can be represented by ladder circuits whose transfer functions contain no zeros in the right half plane, and the seismometer in the bridge is also a ladder circuit when and only when the bridge is perfectly balanced. The transfer function of the seismometer has two zeros at $s = 0$ and $s = \infty$ which are singularities of $\ln F_S(s)$, but it can be shown (Papoulis, 1962) that for zeros of $F(s)$ on the ω axis itself, the Hilbert transforms are still applicable.

4.4 Method of Integration

Due to the singularities ($u = 0, \omega, \infty$), formula (4.4) is difficult to integrate. The numerical integration procedure used is based on an alternative formula proposed by Bode (1945) which reduces the number of singularities to one. A new variable is introduced:

$$x = \ln(u/\omega) \tag{4.7}$$

After integration by parts (Solodovnikov, 1960), the Hilbert transform takes the form:

$$\Phi(\omega) = \frac{1}{\pi}\int_{-\infty}^{+\infty} \frac{dL(x)}{dx} \ln \coth\left|\frac{x}{2}\right| dx \tag{4.8}$$

Since the integration includes the complete frequency spectrum, the phase characteristic at any point depends upon the slope of the gain characteristic in all parts of the spectrum. The relative importance of the slope is given by the weighting factor $\ln \coth \left|\frac{x}{2}\right|$ which becomes logarithmically infinite at $x = 0$ and goes to zero as x becomes large. The integral of the weighting factor is already known (Bode, 1945) and is $\pi^2/2$. Therefore the asymptotic behaviour of the phase is simply the slope of the corresponding asymptote multiplied by $\pi/2$. (Fig. 17)

For numerical integration it is possible to obtain a smooth integrand by subtracting the singularity at x = 0. Equation (4.8) is now written as:

$$\Phi(\omega) = \frac{1}{\pi}\int_{-\infty}^{+\infty}\left[\frac{dL(x)}{dx} - \left.\frac{dL(x)}{dx}\right|_{x=0}\right]\ln\coth\left|\frac{x}{2}\right| dx + \frac{\pi}{2}\left.\frac{dL(x)}{dx}\right|_{x=0} \qquad (4.9)$$

Fig. 17 shows the form of the logarithmic derivative and the weighting factor in the integrand of (4.9) at $\ln\omega = -2$. It should be noted that under the change of scale from u to x (4.7), the value of $\left.\frac{dL(x)}{dx}\right|_{x=0}$ is the same as $\left.\frac{dL(u)}{d\ln u}\right|_{u=\omega}$. The logarithmic derivative used is that of the velocity sensitivity curve of Fig. 16.

The FORTRAN program for the computation of (4.9) is given in the Appendix. Values of the amplitude in the interval between the left and right asymptotes are used to compute the derivative by the 3-point formula:

$$D_i = \frac{(L_{i+1} - L_{i-1})}{2h} \qquad (4.10)$$

where h is the interval between two consecutive pivotal points. On the asymptotes, the derivatives are generated by the program. After tabulation of the weighting function, the integrations are carried out for each ω by Simpson's composite formula:

$$I = h/3\ (f_0 + 4f_1 + 2f_2 + \ldots + 2f_{n-2} + 4f_{n-1} + f_n) \qquad (4.11)$$

4.5 The Tail Error

The integral (4.9) is evaluated inside finite limits a and b with the error introduced by the neglected part given exactly by:

$$\varepsilon_{ta}(\omega) = -\frac{1}{\pi}\left\{\int_{-\infty}^{a}\left[\frac{dL(x)}{dx} - \left.\frac{dL(x)}{dx}\right|_{x=0}\right]\ln\coth\left|\frac{x}{2}\right| dx + \int_{b}^{\infty}\left[\frac{dL(x)}{dx} - \left.\frac{dL(x)}{dx}\right|_{x=0}\right]\ln\coth\left|\frac{x}{2}\right| dx\right\} \qquad (4.12)$$

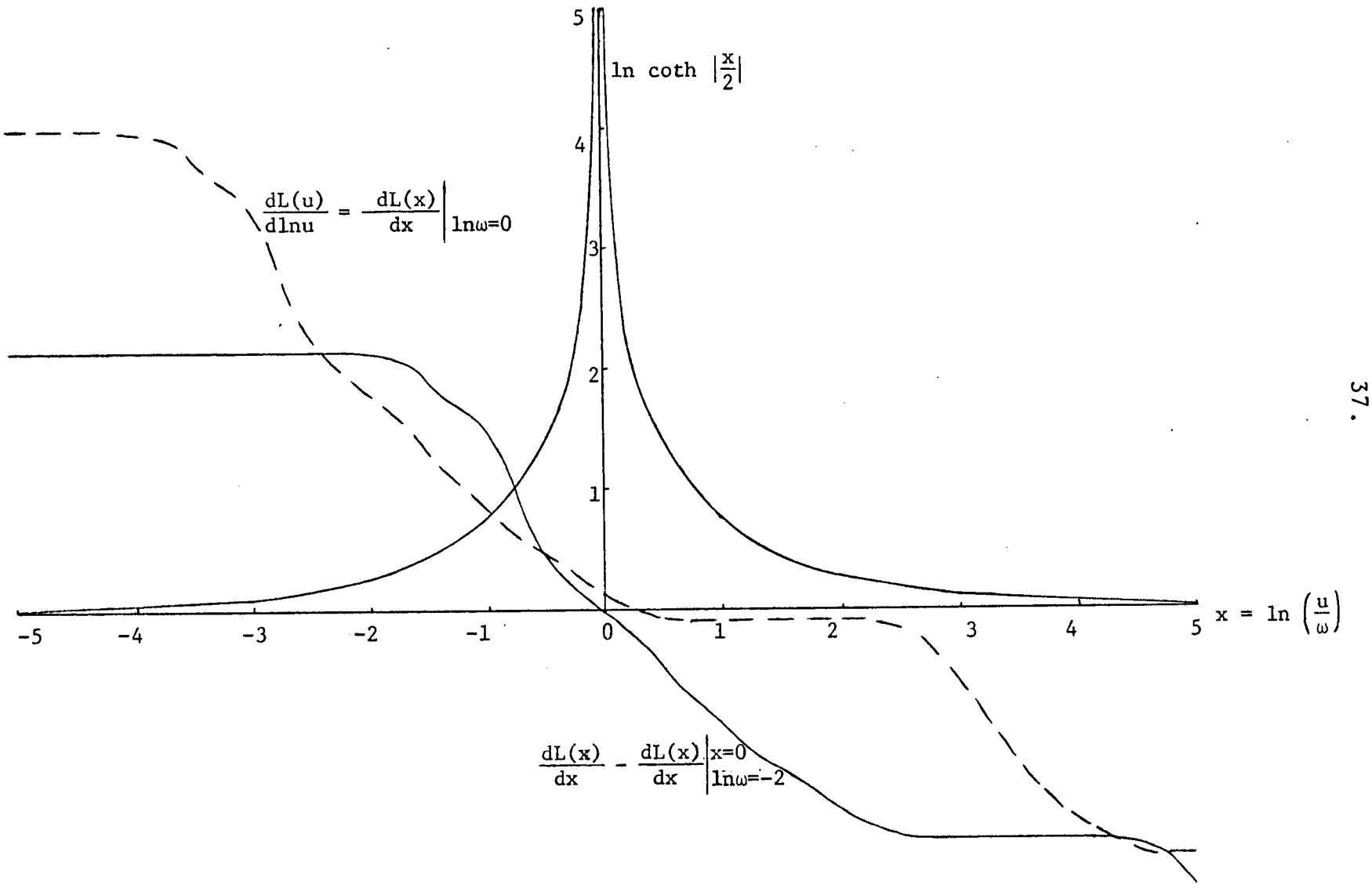

Fig.17 The two components of the integrand of minimum-phase formula (4.9) at $\ln\omega = -2$.

In practice the interval a,b is chosen large enough so that for any ω.:

$$\left.\frac{dL(x)}{dx}\right|_{\substack{x<a \\ \text{all } \omega}} = a_1 \tag{4.13}$$

$$\left.\frac{dL(x)}{dx}\right|_{\substack{x>b \\ \text{all } \omega}} = a_2 \tag{4.14}$$

Choosing a and b with equal absolute values and replacing $\coth\left|\frac{x}{2}\right|$ by its definition, the expression for $\varepsilon_{ta}(\omega)$ reduces to:

$$\varepsilon_{ta}(\omega) = \frac{1}{\pi}\left[2\left.\frac{dL(x)}{dx}\right|_{x=0} - a_1 - a_2\right]\int_b^\infty \ln\frac{e^x+1}{e^x-1}\,dx \tag{4.15}$$

The series expression for the integrand is given by:

$$\ln\frac{e^x+1}{e^x-1} = 2\sum_{k=1}^{\infty}\frac{e^{(1-2k)x}}{(2k-1)} \qquad (x>0) \tag{4.16}$$

Integrating(4.15) term by term yields:

$$\varepsilon_{ta}(\omega) = \frac{2}{\pi}\left[\left.\frac{2dL(x)}{dx}\right|_{x=0} - a_1 - a_2\right]\sum_{k=1}^{\infty}\frac{e^{(1-2k)b}}{(2k-1)^2} \tag{4.17}$$

The series is rapidly converging and when applied to the seismograph curves, the contribution of $\varepsilon_{ta}(\omega)$ is found to be very small (See Sect.4.8). If the conditions (4.13) and (4.14) do not apply, inspection of (4.12) shows that for any configuration an upper bound on the tail error is given by:

$$\left|\varepsilon_{ta}\right|_{max} = \frac{2}{\pi}\left(\left|a_1\right| + \left|a_2\right|\right)\sum_{k=1}^{\infty}\frac{e^{(1-2k)b}}{(2k-1)^2} \tag{4.18}$$

4.6 Truncation and Round-off Errors

An estimate of the truncation error in the differentiation is given by McCormick and Salvadori (1964):

$$\varepsilon'_{tr} = \frac{h^2}{6} f^{(3)}(\xi) \tag{4.19}$$

For each double interval of integration, a similar estimate is given by McCormick and Salvadori (1964):

$$\varepsilon_{tr} = \frac{h^5}{90} f^{(4)}(\xi) \tag{4.20}$$

where $f^{(i)}(\xi)$ are the higher order derivatives evaluated within the interval. These errors are determined by the choice of interval at which one reads the amplitude values from the Bode plot.

The program was tested with systems described by analytical functions and the computed phase was compared with the true phase for different values of h. It appears that the choice of h is not particularly critical provided it is not extreme. The value of 0.2 was used. A worked out example will show how the errors propagate.

The system chosen is the normalized second order system with damping ratio equal to one. In the frequency domain the gain and phase are given respectively by:

$$A(u) = \left(\frac{1}{1 + u^2}\right) \tag{4.21}$$

$$\Phi(u) = \tan^{-1}\left(\frac{2u}{1-u^2}\right) \tag{4.22}$$

On the Bode plot the variables are changed from linear to logarithmic and the gain and its derivative become:

$$L(u) = \ln \frac{1}{1 + e^{2\ln u}} \tag{4.23}$$

$$\frac{dL(u)}{d\ln u} = \frac{-2}{1 + e^{-2\ln u}} \tag{4.24}$$

The logarithmic gain L(u) has a corner at u = 1 and the slopes of the left and right asymptotes are respectively 0 and -2. Further inspection of (4.24) shows that the slope is exactly -1 at ln u = 0 (u=1) and completely symmetrical relative to that point. With the limits of integration fixed at a = -10 and b = +10, the phase response will be computed from $x_{min} = -7$ ($x_{min} = \ln\omega_{min}$) to $x_{max} = +7$ ($x_{max} = \ln\omega_{max}$) which corresponds to a lower frequency of 1.45×10^{-4} hz and an upper frequency of 1.75×10^{2} hz. The logarithmic derivative at each point is given exactly by (4.24) and will be kept at seven significant digits to eliminate the input errors which will be considered in the next section.

Because of the symmetry of $\frac{dL(u)}{d\ln u}$ one can readily see that the phase should be exactly 0 at ω=1 as should the tail and truncation errors. Moreover, these errors should also show symmetry relative to ω=1. The actual results are presented in Fig. 18 and Fig. 19.

The results for both the phase and the error are those expected with their values at ω=1 slightly different from zero due to roundoff error. The limit on the tail error given by (4.18) amounts to:

$$\left|\varepsilon_{ta}\right|_{max} = \frac{2}{\pi}(0 + 2)(e^{-10}) = .0000578\text{rad} = .00331\text{deg}. \tag{4.25}$$

The error in Fig. 19 tends to that value at the extremities of the spectrum. This was also expected since for small or large values of ω (relative to ω=1) the contribution of the integral in (4.9) becomes zero leaving only the

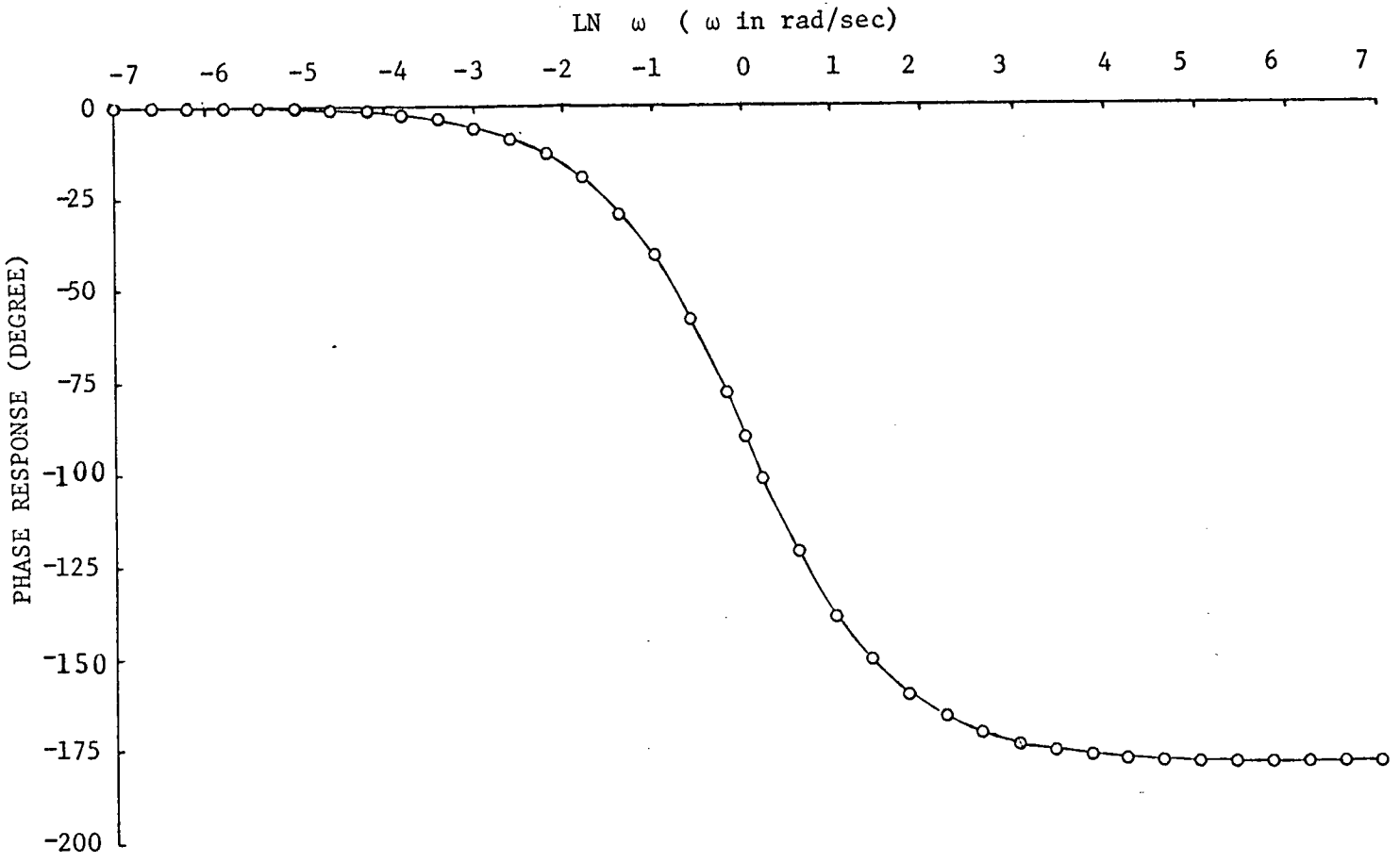

Fig. 18 Phase response of the normalized second order system computed using minimum-phase program.

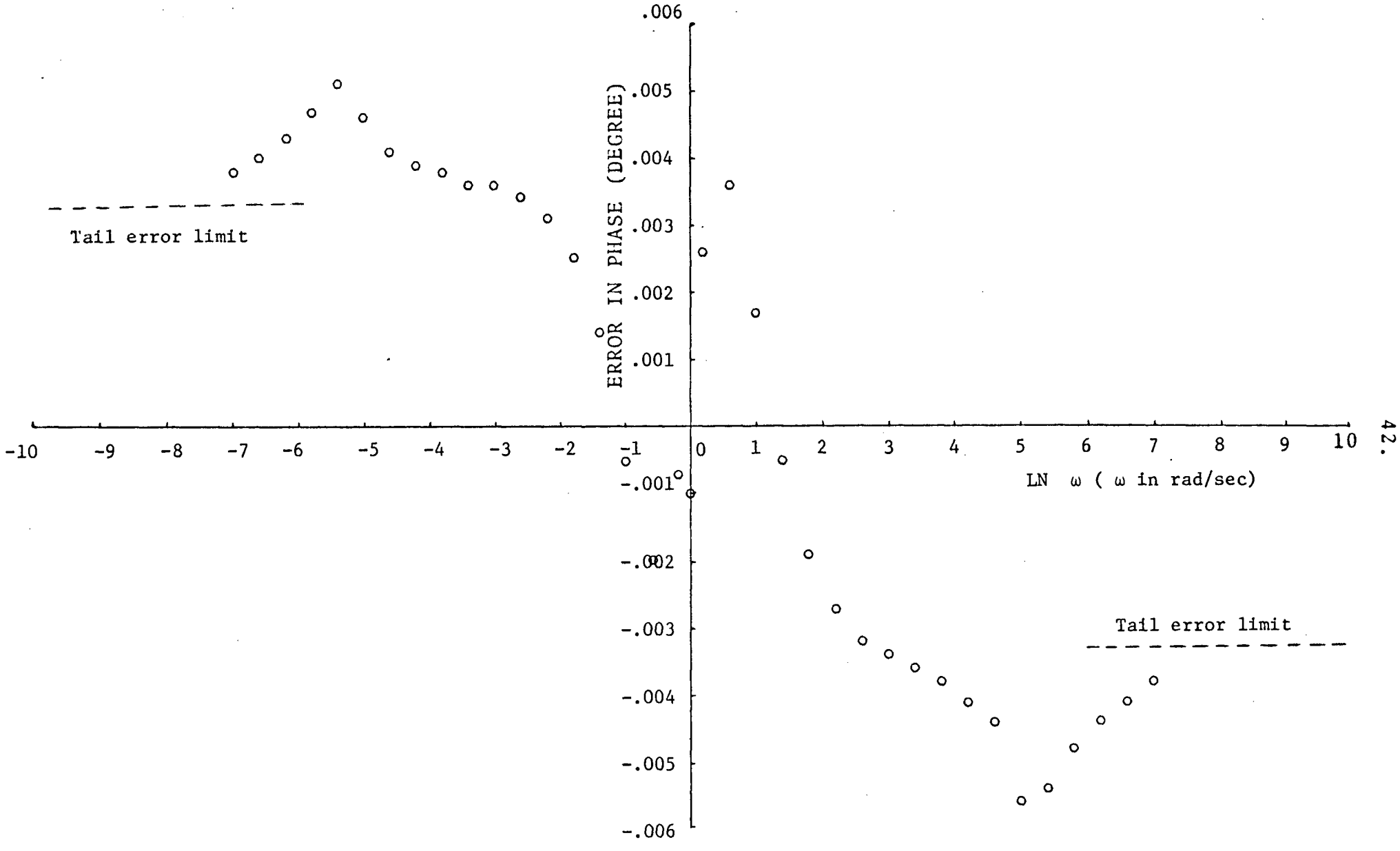

Fig.19 Error in the phase response of the normalized second order system for a seven significant digits logarithmic amplitude.

tail error. Furthermore, the maximum absolute value of ε is .0056; it shows that the truncation and roundoff errors are very small. Similar results were obtained using other analytical systems. It is concluded that these errors are completely negligible compared to errors introduced by uncertainties in the data.

4.7 Effects of Errors in the Amplitude Data

Formula (4.9) is composed of two terms and since the algorithm for numerical differentiation magnifies input errors more than the algorithm for numerical integration, it might appear at first sight that the main source of error would come from the $\frac{\pi}{2}\frac{dL(x)}{dx}\Big|_{x=0}$ term. However, if an uncertainty δ_o is assumed for the derivative term at $x=0$, the error ε_o' is zero due to cancellation by the integral term:

$$\varepsilon_o' = -\frac{1}{\pi}\int_{-\infty}^{+\infty}\left[\frac{dL(x)}{dx}\Big|_{x=0} + \delta_o\right] \ln \coth\left|\frac{x}{2}\right| \, dx + \frac{\pi}{2}\left[\frac{dL(x)}{dx}\Big|_{x=0} + \delta_o\right] = 0 \quad (4.26)$$

The error arises from the integral term only and is expected to be small due to the smoothing effect of integration. More explicit consideration will be presented now.

In practice, a smooth curve is traced on the Bode plot through the unequally spaced amplitude points and the input data are obtained by reading this curve at the chosen interval of 0.2 unit. If a new curve is drawn from a different series of measurements performed under the same conditions, it is found to fit the original one to at least two significant digits accuracy.

The method was tested once again with a system whose answer is known but this time by reading the amplitude with only two significant digits. Fig. 20 shows the errors obtained for the second order system studied in section 4.6. Even at this low degree of accuracy

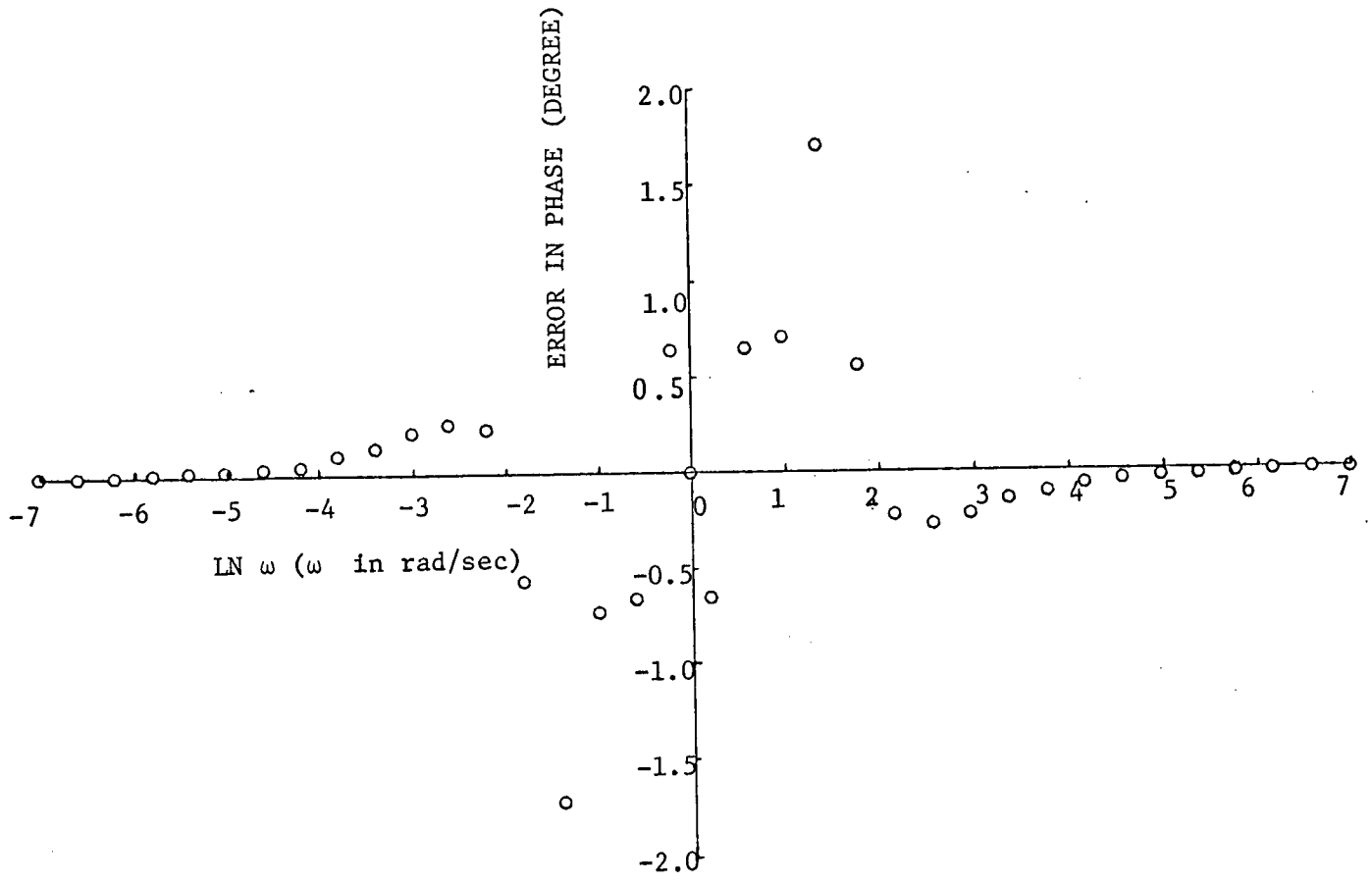

Fig. 20 Error in the phase response of the normalized second order system for a two significant digits logarithmic amplitude.

on the amplitude, the maximum error that can be found is 1.71 degree and that only for two of the frequencies, the average error being much smaller. The method was also tested with first and third order systems in the same manner and an error as large as two degrees never appeared.

The seismograph curves are quite similar to these theoretical curves; they are also smooth and monotonically decreasing and they behave as fourth and second order systems at low frequencies, and as second order systems at higher frequencies (Fig. 17). They are known to at least two significant digits and on a sufficiently wide band to determine the position of their asymptotes. It is believed that the error on the phase calculated by this method is at most ±2°, with ±1° likely to be a more realistic figure.

4.8 The Phase Response

The phase response was found by the method described above for the Sprengnether and the Geotech at the temperatures that brought their equilibrium position to -6mm, 0mm and +6mm. The limits of integration were reduced to a = -7 and b = +7 which gives a maximum tail error of about .05 degree for a seismograph curve. The resonances of the Sprengnether (Fig. 15) are not taken into account since they appear outside the range of the frequencies of interest, that is, far from the large values of the weighting factor and further their contributions to the remaining part of the integral largely cancel because of the rapidly oscillating character of the derivative in that region.

The transfer function of the amplifier is therefore used beyond $\ln u = 2.6$.

The corner frequency of the recorder is not visible on the velocity sensitivity curves because of the wide band response of the Brush 480 (f_H = 125 cps). Negligible error is introduced by neglecting its effect. It should be noted that an error which multiplies the whole set of points by a certain value e.g. an error in the determination of the constants of the seismometer (see 3.13), does not affect the logarithmic derivative.

The results for periods between 100 sec. and 1 sec. are collected in Table II and Table III. The phase responses at the center position of the seismometer scales are plotted on Fig. 21 and Fig. 22. The circular points on these figures represent experimental values obtained by measuring the phase difference by zero-crossing between the voltage applied to the bridge (acceleration) and the output voltage from the seismograph. The phase shift of the velocity is obtained by adding 90°. The Δ columns of Table II and Table III represent the difference in the phase response at ±6mm relative to the phase response at 0mm. It can be seen that the region most affected by the zero instability is the band between 5 sec. and 100 sec. This represents two octaves on each side of the natural frequency of the seismomter. It is the region where the slope of the transfer function of the seismometer, i.e. the derivative of (3.7) is most affected by a change in its constants. The other parts of the curve largely depend on the amplifier-recorder slopes and should not be much disturbed by a change in the mass position of the seismometer

For the Sprengnether the change in phase response is about 3° and for the Geotech, it is about 2° on one side and 4° on the other. This is a significant change and points out the necessity of keeping

ln ω	F (hz)	T (sec)	Δ_{-6mm} (degree)	Φ (degree)	Δ_{+6mm} (degree)
-2.8	.010	103.3	0	240	3
-2.6	.011	84.6	-2	222	2
-2.4	.014	69.3	-2	204	3
-2.2	.018	56.7	-3	188	3
-2.0	.022	46.4	-4	172	3
-1.8	.026	38.0	-3	155	4
-1.6	.032	31.1	-5	140	3
-1.4	.039	25.5	-4	123	3
-1.2	.048	20.9	-3	106	3
-1.0	.058	17.1	-4	91	2
-0.8	.072	14.0	-3	76	2
-0.6	.087	11.4	-2	62	3
-0.4	.107	9.4	-1	50	2
-0.2	.130	7.7	-1	40	1
0.0	.159	6.3	0	31	1
0.2	.194	5.1	0	24	1
0.4	.237	4.2	0	18	0
0.6	.290	3.4	0	13	0
0.8	.354	2.8	0	8	1
1.0	.433	2.3	0	4	1
1.2	.528	1.9	0	0	1
1.4	.645	1.6	0	-3	0
1.6	.788	1.3	1	-8	1
1.8	.963	1.0	0	-12	0
2.0	1.176	0.8	0	-17	1

Table II. The phase response of the Sprengnether-SSA combination: Φ-the phase shift, center position; Δ columns represent the difference from Φ for the mass at ±6mm.

ln	F (hz)	T (sec)	Δ_{-6mm} (degree)	Φ (degree)	Δ_{+6mm} (degree)
-2.8	.010	103.3	-2	246	-8
-2.6	.011	84.6	1	225	-7
-2.4	.014	69.3	1	206	-4
-2.2	.018	56.7	1	189	-2
-2.0	.022	46.4	1	173	1
-1.8	.026	38.0	2	157	2
-1.6	.032	31.1	4	140	4
-1.4	.039	25.5	4	124	4
-1.2	.048	20.9	2	109	2
-1.0	.058	17.1	1	94	-1
-0.8	.072	14.0	-2	81	-4
-0.6	.087	11.4	-4	69	-7
-0.4	.107	9.4	-4	57	-8
-0.2	.130	7.7	-4	46	-7
0.0	.159	6.3	-3	36	-6
0.2	.194	5.1	-2	27	-4
0.4	.237	4.2	-1	20	-3
0.6	.290	3.4	-1	15	-3
0.8	.354	2.8	-1	10	-2
1.0	.433	2.3	-1	6	-2
1.2	.528	1.9	-1	2	-2
1.4	.645	1.6	0	-3	-1
1.6	.788	1.3	0	-7	-1
1.8	.963	1.0	0	-11	-1
2.0	1.176	0.8	0	-16	-2

Table III. The phase response of the Geotech-SSA combination: Φ-the phase shift, center position; Δ columns represent the difference from Φ for the mass at ±6mm.

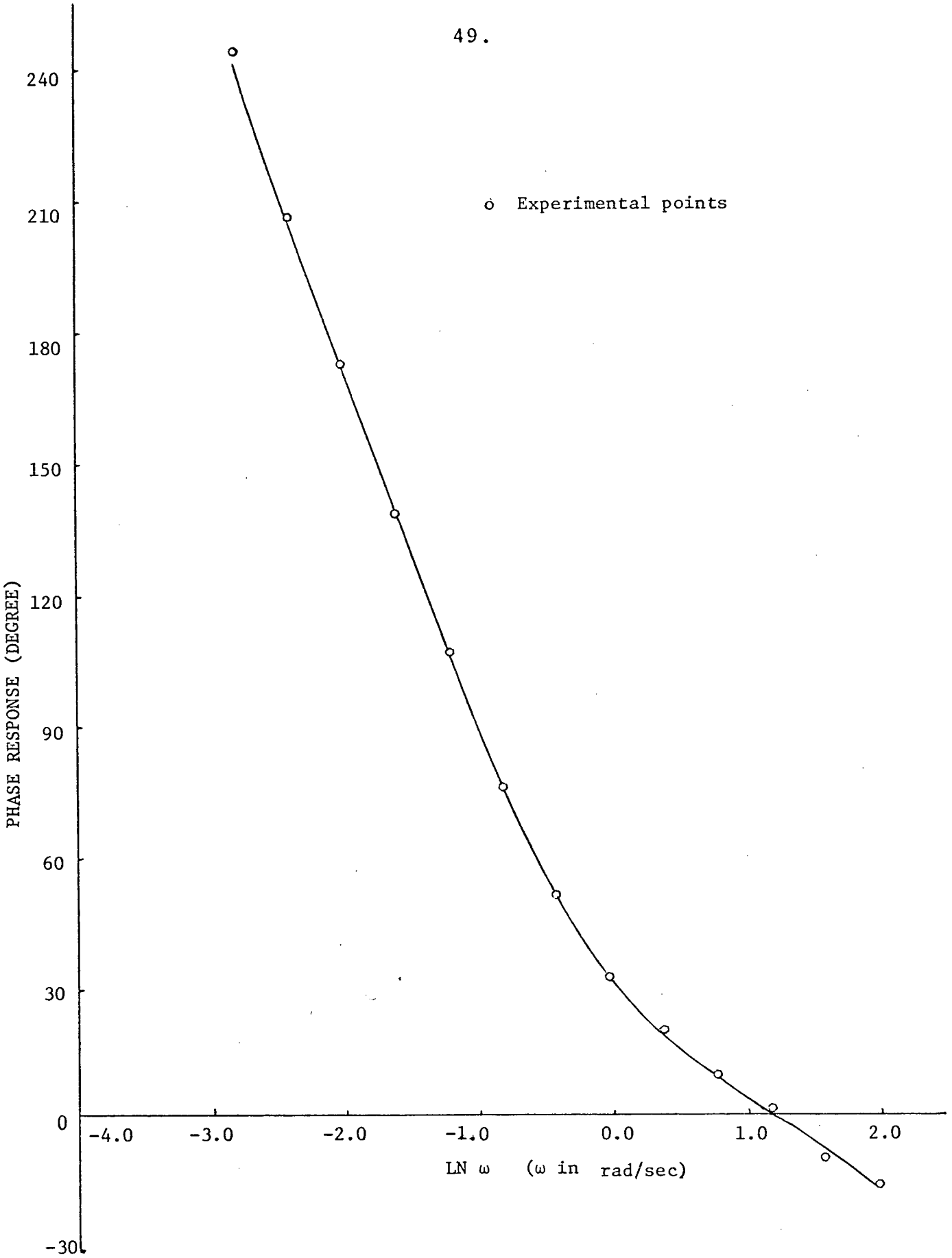

Fig. 21 Phase response of the Sprengnether seismometer-solid state amplifier(SSA) combination at center position.

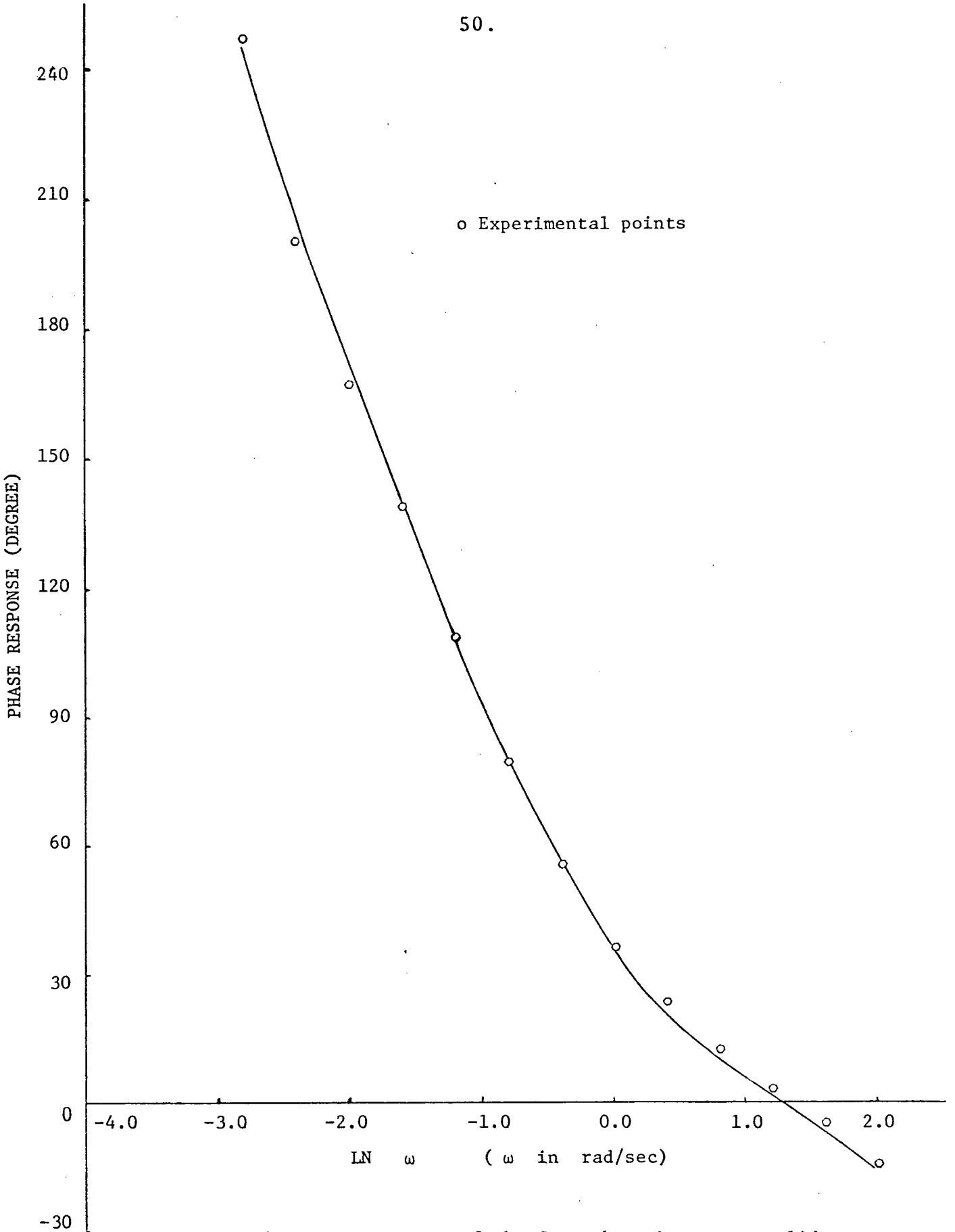

Fig. 22 Phase response of the Geotech seismometer-solid state amplifier (SSA) combination at center position.

the seismometer in a stable temperature environment. It has been observed that the amplitude response does not vary linearly with the deviation of the mass from the zero position, but that the rate of change increases. For a ±3 mm drift, which corresponds to a temperature fluctuation of less than 1°C, the phase change can be held to less than 1.5° provided the unsymmetrical response of the Geotech can be corrected. It is expected that this standard can be achieved with an improved temperature controller.

The geophysical implications of these errors will be discussed in Chapter VI.

Chapter V

The Noise

5.1 The Thermal Noise

A fundamental theorem due to Nyquist (1928) states that a noise source results from thermal agitation associated with any dissipative element of an electrical network. This source can be represented by an rms voltage $\overline{V}$ in series with the output impedance Z_o (admittance Y_o) of the equivalent electrical circuit or by an rms current $\overline{I}$ across the same impedance. The corresponding spectral densities are given by:

$$G_{nV} = 4kTRe(Z_o) \tag{5.1}$$

$$G_{nI} = 4kTRe(Y_o) \tag{5.2}$$

where:

k = Boltzman's constant

T = absolute temperature

As pointed out by Russell and Kollar (1966) in their analysis of a "mass on a spring" seismometer, the source current analysis can be made with ease. From the circuit of Fig. 5, $Re(Y_o)$ is simply the damping resistor (R is parallel with R_D) in the parallel resonant circuit and is independent of frequency.

At long periods, the terms ℓ, ℓ' and r' are completely negligible. Referring to the circuit of Fig. 5 and using (2.28), the mean square current across the damping resistor is equivalent to:

$$\overline{I}^2 = \frac{K^2 \overline{v}^2}{l_p^2 G^2} \tag{5.3}$$

Moreover:

$$\overline{I}^2 = \int_{f_1}^{f_2} G_{nI}\, df \tag{5.4}$$

Combining (5.2), (5.3) and (5.4) and substituting s^2y for $\ddot{y}$:

$$\overline{y_1^2} = \left(\frac{1_p G}{2\pi^2 K}\right)^2 \frac{kT(R+R_D)}{RR_D} \int_{f_1}^{f_2} \frac{df}{f^4} \tag{5.5}$$

For a bandwidth of one octave about a central frequency f, the lower limit f_1 is equal to $f/\sqrt{2}$ and the upper limit is equal to $\sqrt{2}\,f$. With these limits, equation (5.5) becomes:

$$\overline{y_1}^2 = \frac{7\sqrt{2}\; 1_p^2 kT(G^2 + DR_D)}{48\pi^4 K^2 R_D f^3} \tag{5.6}$$

For comparison with seismic noise, it is more convenient to express the equivalent ground displacement as a peak-to-peak amplitude. The peak is taken as that value whose magnitude is exceeded 5% of the time. For this definition, the ratio of peak-to-peak amplitude to rms value is 3.28 (Byrne, 1961). In microns:

$$y_{PP_1} = \frac{3.28\times10^6 1_p}{4\pi^2 K} \left[\frac{7\sqrt{2}\; kT(G^2+DR_D)}{3R_D f^3}\right]^{1/2} \tag{5.7}$$

5.2 The Excess Noise

Usually, the noise measured at the output of an amplifier is much higher than the thermal noise of the input resistance. Many sources are responsible for this excess noise and it is common in electronics to represent it by an equivalent rms voltage source in series with the input resistance of the amplifier. A corresponding spectral density of the ground displacement, G_{ne}, may be obtained by dividing the spectral density of the excess noise G_e at the input of the amplifier by the square of the magnification of the seismometer:

$$G_{ne} = \frac{G_e}{|sF_S|^2} \tag{5.8}$$

From (3.7):

$$G_{ne} = \frac{G_e 1_p^2}{64\pi^6 G^2 K^2 Z_i^2}\left[\frac{16\pi^4 K^2 R_D^2}{f^2} + \frac{4\pi^2(G^4+2DR_DG^2-2KR_D^2U+D^2R_D^2)}{f^4} + \frac{R_D^2U^2}{f^6}\right] \quad (5.9)$$

For one octave bandwidth around f, the corresponding peak-to-peak ground amplitude, in microns, is given by:

$$y_{pp_2} = \frac{3.28\times10^6 1_p}{8\pi^3 GKZ_i}\left\{G_e\left[\frac{8\sqrt{2}\pi^4 K^2 R_D^2}{f} + \frac{7\sqrt{2}\pi^2(G^4+2DR_DG^2-2KR_D^2U+D^2R_D^2)}{3f^3} + \frac{31\sqrt{2}\,R_D^2U^2}{40f^5}\right]\right\}^{1/2} \quad (5.10)$$

5.3 The Noise Spectrum of the Amplifier

To determine the noise introduced by the amplification stage exclusive of the long-period seismometer, the spectra of the PTA and SSA amplifiers were measured. The spectra G_A were obtained by taking the Fourier transform of the time autocorrelation function of the noise N(t):

$$G_A(f) = \lim_{T\to\infty}\frac{1}{T}\int_{-\infty-T/2}^{+\infty+T/2} N(t)N(t+\tau)e^{-j2\pi f\tau}\,dt\,d\tau \quad (5.11)$$

The signal from the amplifier was recorded digitally and standard techniques used to evaluate (5.11). The band of the signal was limited by the low cutoff frequency of the amplifier ($\simeq$.01 hz) and the high cutoff frequency of the digital voltmeter ($\simeq$1.5 hz) which was sampling at an interval of 0.14 sec. A one hour record length was used to obtain sufficient precision for the long-period components. The spectrum of the PTA at any gain (the attenuator is at the input of the amplifier) with an input of 40Ω is shown in Fig.23. The

spectrum of the SSA (Gain: 100000) with an input resistance of 300Ω is shown in Fig. 24. In both cases, the spectrum was smoothed by tapering the autocorrelation function with a Hanning window.

5.4 Comparison with Seismic Noise

Statistical data on microseismic noise has been collected by Brune and Oliver (1959). Their results are summarized by three curves representing maximum, average, and minimum values of surface displacement in a one octave bandwidth (solid portion of upper 3 curves in Fig. 25 and 26). Savino and Hade (1970) and Savino et al (1971) have observed a pronounced minimum in the spectrum of earth noise between 30 and 40 sec and an increase of 14 db/octave noise between 50 to 100 sec at Ogdensburg, N.J. Similar results are found elsewhere in the world. This increase in noise is attributed to loading of the earth's surface by atmospheric pressure variations. On this basis the curves of Brune and Oliver are continued to longer periods in Fig. 25 and 26 (dotted sections of curves).

To determine whether microseismic or instrument noise predominates at a given frequency, the curves for earth noise are compared with the apparent noise at the surface of the earth due to the fundamental thermal noise of the seismometer and the excess noise of the SSA amplifier (Gain=3000) for both the Sprengnether (Fig. 25) and Geotech (Fig. 26).

Curve 1 is obtained directly from equation (5.7) using the values of Table I for the center position. Curve 2a is obtained from equation (5.10) where G_e is the average spectral density given by the mean square noise divided by the bandwidth of the noise and referred to the input of the amplifier:

$$G_e = \frac{\overline{N}^2}{\text{Gain}^2 \Delta f} \qquad (5.12)$$

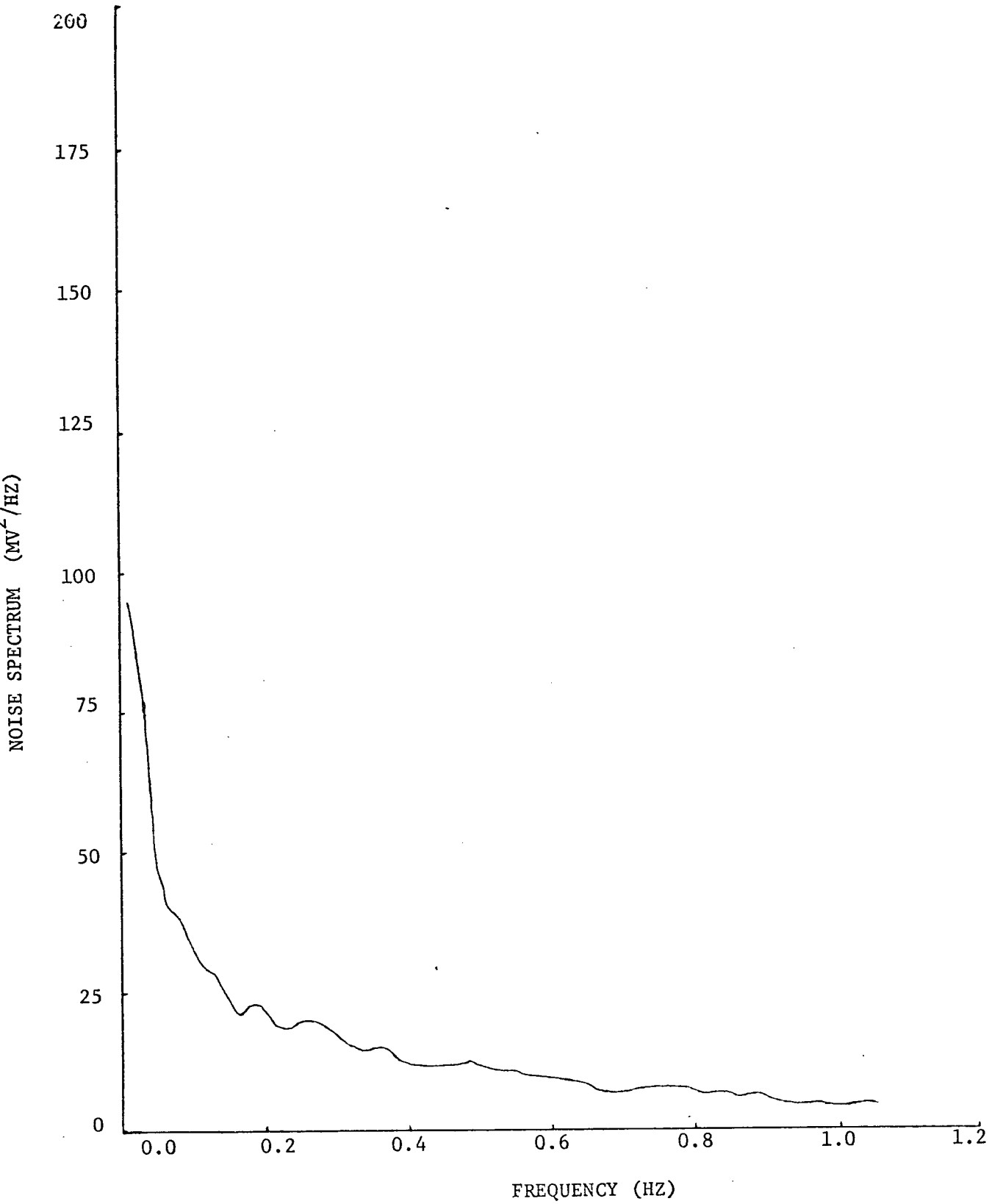

Fig. 23 Noise spectrum of the Geotech phototube amplifier (PTA) with 40Ω input resistance at any gain.

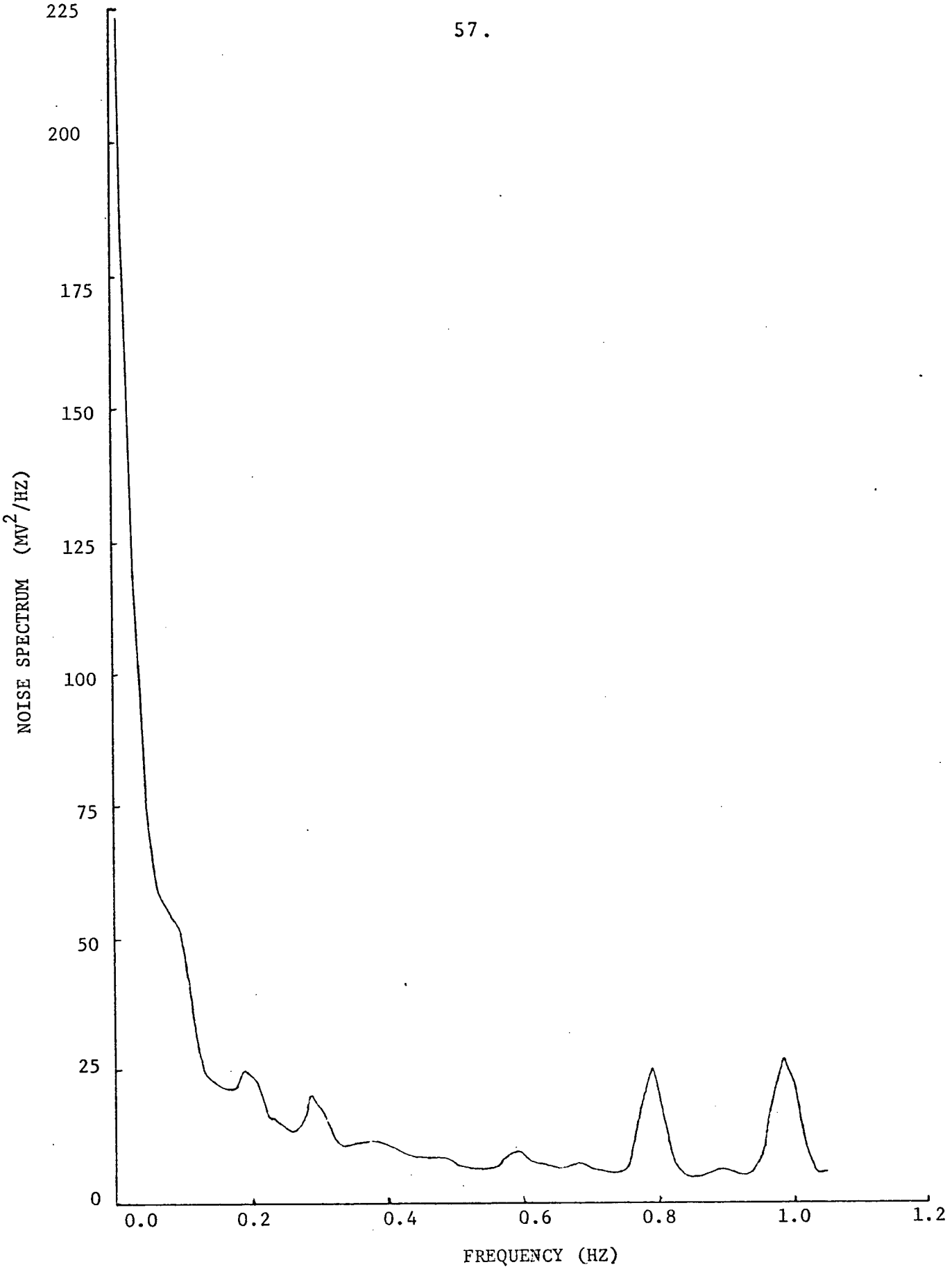

Fig. 24 Noise spectrum of the Geotech solid state amplifier (SSA) with 300Ω input resistance at 100000 gain.

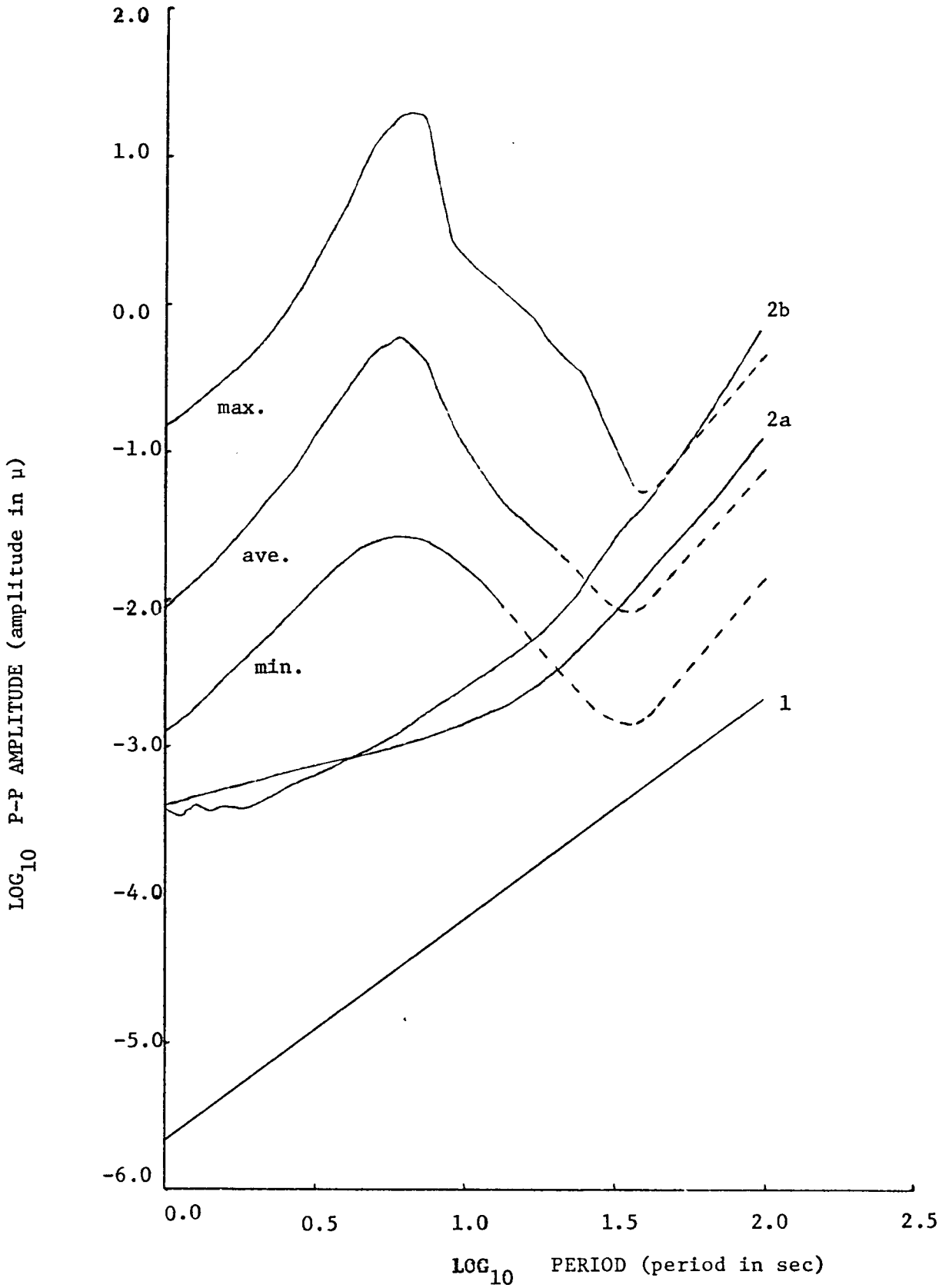

Fig. 25 Comparison of seismic noise with the fundamental noise(1) of the Sprengnether seismometer and the excess noise (2) of the solid state amplifier (SSA). 2a is determined from 5.10; 2b is obtained from the SSA spectrum.

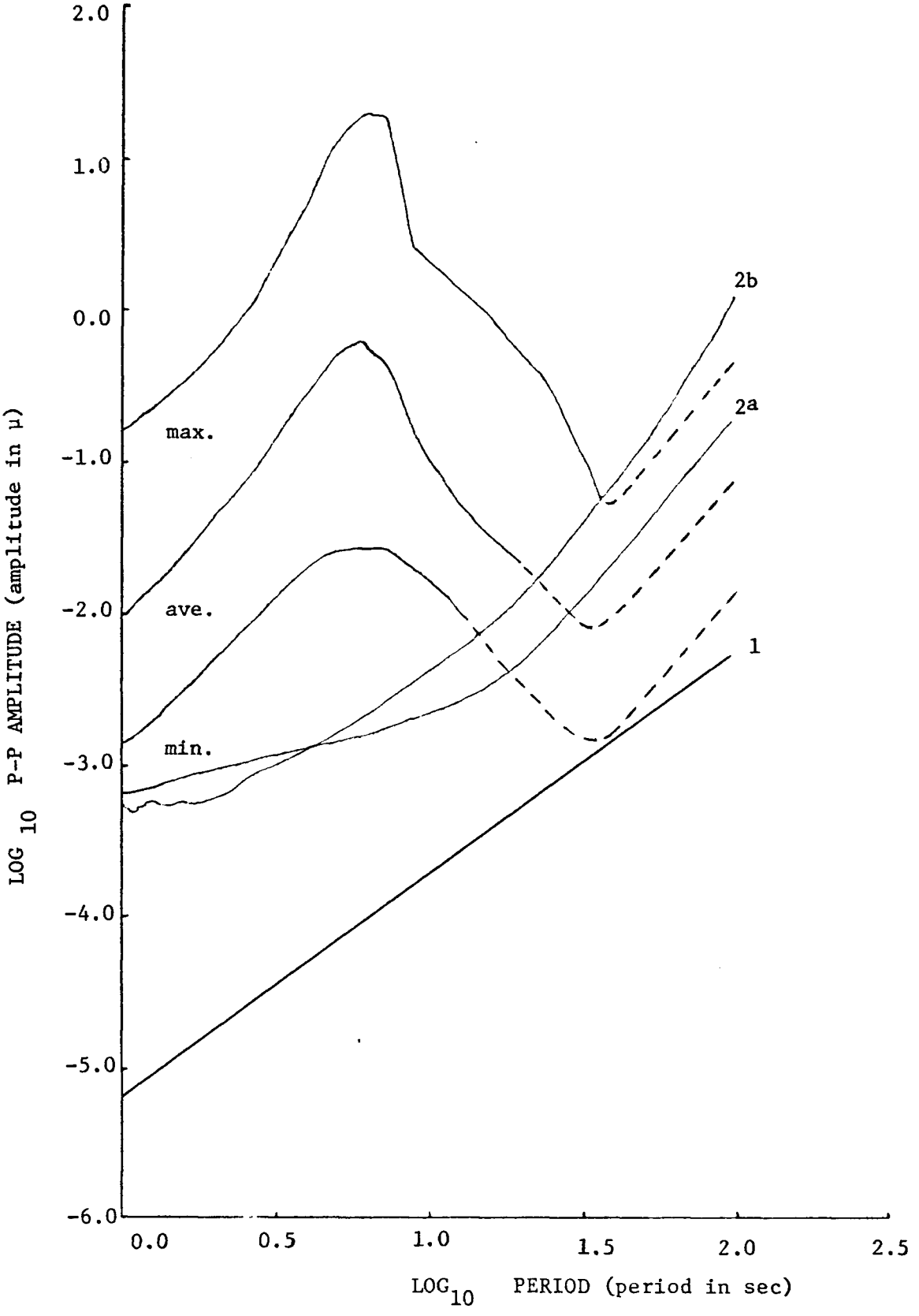

Fig. 26 Comparison of seismic noise with the fundamental noise(1) of the Geotech seismometer and the excess noise(2) of the solid state amplifier (SSA). 2a is determined from 5.10; 2b is obtained from the SSA spectrum.

The mean square noise at the output of the SSA corresponds to the zero lag autocorrelation function and is equal to 34.3 mV^2. For a gain of 100000 and a bandwidth of 1.5 cps, the average spectral density is 2.28×10^{-15} V^2s. From this, the spectral density of the fundamental noise at the input of the amplifier must be subtracted, it is equal to $4kTR_i$ or $5.28 \times 10^{-18} V^2s$. Since it is three orders lower than G_e, it can be considered negligible and all the output noise is excess noise.

The spectra of Fig. 23 and Fig. 24 are not exactly white, in particular at low frequencies, where the 1/f component dominates. Curve 2b is a better estimate of the corresponding ground displacement. It is obtained by a numerical integration of the SSA spectrum divided by the square of the magnification curves of the Sprengnether and the Geotech. Because of the changing limits of integration, it is easier to do this integration on a $\log_{10} f$ scale.

On that scale:

$$y_{pp_2} = 3.28 \times 10^6 \left[9 \times 10^{-4} \ln 10 \int_{x-.15}^{x+.15} \frac{G_A(x) 10^x dx}{MS(x)^2} \right]^{1/2} \qquad (5.13)$$

The 9×10^{-4} factor is to scale the power spectrum to the amplification level of the SSA (3000) used in the measurement of the magnification MS.

From the curves of Fig. 25 and Fig. 26, one can conclude that the fundamental noise of the seismometer-amplifier combination (without filter) is negligible in comparison with the excess noise of the SSA amplifier. The excess noise should be of the same order as the seismic noise at longer periods and less important at periods below the 30-40 sec minimum. For any period the sum of all noises is equal to:

$$y = \sqrt{y_{pp_1}^2 + y_{pp_2}^2 + y_{seismic}^2} \tag{5.14}$$

In the above discussion it is assumed that the seismometer cases are airtight and perfectly rigid i.e. pressure effects have not been considered.

Chapter VI

Summary and Conclusions

6.1 Reliability of Phase Velocity

In phase velocity measurements, the phase shift $\Delta\Phi(\omega)$ of a component of the wavetrain spectrum over a known distance Δx is related to the travel time by:

$$\Delta\Phi = \omega\Delta t \tag{6.1}$$

The phase velocity $c(\omega)$ is given by:

$$c = \frac{\Delta x}{\Delta t} \tag{6.2}$$

$$= \omega\frac{\Delta x}{\Delta\Phi} \tag{6.3}$$

When measuring $\Delta\Phi$, the phase shift introduced by the seismograph must be subtracted at both stations. As the phase response of the instruments are known only within certain limits, it is important to determine the error in phase velocity due to errors in the phase response. By (6.3)

$$dc = \frac{\omega\Delta x}{\Delta\Phi^2}\, d\Delta\Phi \tag{6.4}$$

$$= \frac{c^2 T}{2\pi\Delta x}\, d\Delta\Phi \tag{6.5}$$

Assuming that the instrumental phase at one station can be determined to $\pm 2°$, and allowing an additional degree for phase inaccuracies due to temperature fluctuations, the most probable error for 2-station measurements is given by:

$$d\Delta\Phi = \pm \frac{2\pi\sqrt{2(2^2 + 1^2)}}{360} \tag{6.6}$$

$$= \pm\ 0.055 \tag{6.7}$$

For a two significant digit velocity determination, we have by (6.5):

$$\frac{c^2 T}{2\pi\Delta x} < 1$$

At 20 sec period this requires for typical velocities a station separation of only 40 km but at 80 sec a separation of 200 km is required to achieve this accuracy. Some errors may also be introduced by geologic effects (e.g. refraction) and analysis procedures.

6.2 Environmental Problems

In this feasability study of a portable long period seismic array, it is found that achievement of temperature stability to within 1°C is necessary. Fluctuations larger than this lead to changes in the instrumental phase response in excess of 1°.

Large pressure fluctuations (2 cm Hg) will not influence the zero stability significantly. Rapid fluctuations may however be a noise source if the seismometer case is not airtight or if it is not sufficiently rigid. The seismometer should be located in an environment where short term fluctuations are minimized.

6.3 Noise

At the periods of interest for Rayleigh wave studies, the instrumental and seismic noiseare of the same order. The fundamental noise is not significant although it will increase when filters are introduced to shape the seismograph responses to give maximum sensitivity in the 50 to 100 sec band.

6.4 Determination of Phase Response from the Amplitude Response

For a minimum-phase system, determination of the phase response from the amplitude response has been shown to be feasible. However, the amplitude response is required over a much wider frequency band than the region of interest of $\Phi(\omega)$. In the particular systems under consideration, this has lead to several problems; calibration due to eddy currents, noise levels, and resonances in the system. For the portable system , it is recommended that the phase response of the system be determined directly. However, it is expected that the techniques given here will be useful when only the amplitude curves are available as in the case for many permanent stations. Further these procedures serve as an aid to relate the form of the phase response to the basic physical characteristics of the system.

References

Bode, H.W., Network analysis and feedback amplifier design, D. van Nostrand Co., Inc., New York, N.Y., 1945.

Brune, J.N. and J. Oliver, The seismic noise of the earth's surface, Bull. Seism. Soc. Am., 49, 349-353, 1959.

Byrne, C.J., Instrument noise in seismometers, Bull. Seism. Soc. Am., 51, 69-84, 1961.

Caner, B., Electrical conductivity structure in Western Canada and petrological interpretation, J. Geomagn. Geoelectr., 22, 113-129, 1970.

Dorman, J. and M.Ewing, Numerical inversion of seismic surface wave dispersion data and crust-mantle structure in the New York-Pennsylvania area, J. Geophys. Res., 67, 5227-5241, 1962.

Haskell, N.A., The dispersion of surface waves in multilayered media, Bull. Seism. Soc. Am., 43, 17-34, 1953.

Isacks, B. J., J. Oliver, and L.R. Sykes, Seismology and the new global tectonics, J. Geophys. Res., 73, 5855-5899, 1968.

Kollar, F. and R. D. Russell, Seismometer analysis using an electric current analog, Bull. Seism. Soc. Am., 56, 1193-1205, 1966.

McCormick, J. M. and M.G. Salvadori, Numerical methods in FORTRAN, Prentice-Hall, Inc., Englewood Cliffs, N.J., 1964.

McGarr, A. and L. Alsop, Transmission and reflection of Rayleigh waves at vertical boundaries, J. Geophys. Res., 72, 2169-2180, 1967.

Mal, A. K. and L. Knopoff, Transmission of Rayleigh waves past a step change in elevation, Bull. Seism. Soc. Am., 55, 319-334, 1965.

Melton, B. S., Technical note 2/70, The La Coste suspension-Principles and practice, Teledyne Geotech, 3401 Shiloh Road, Garland, Texas, 1970.

Nyquist, H., Thermal agitation of electric charge in conductors, Phys. Rev., 32, 110-113, 1928.

Papoulis, A., The Fourier integral and its applications, McGraw-Hill Book Co., Inc., New York, N.Y., 1962.

Pilant, W. L. and L. Knopoff, Observations of multiple seismic events, Bull. Seism. Soc. Am., 54, 19-39, 1965.

Sato, Y., Analysis of dispersed surface waves by means of Fourier Transform I, Bull. Earthq. Res. Inst., 33, 33-50, 1955.

Savino, J. and G. Hade, Long-period (15-150 sec) seismic noise observations at the Ogdensburg Mine Observatory, Trans. Amer. Geophys. Union, 574, 1970.

Savino, J., K. McCamy and G. Hade, An improved high-gain, long-period, seismograph system, III. A pronounced minimum in the spectrum of long-period earth noise between 30 and 40 sec., Trans. Amer. Geophys. Union, 558, 1971.

Shima, E., Theoretical and experimental approach to the designs and calibrations of electro-magnetic seismograph: I. Voltage sensitivity of the moving-coil type seismometer, Bull. Earthq. Res. Inst., 38, 29-39, 1960.

Solodovnikov, V.V., Introduction to the statistical dynamics of automatic control systems, Dover Publication Inc., New York, N.Y., 1960.

White, W. R. H. and J. C. Savage, A seismic refraction and gravity study of the earth's crust in British Columbia, Bull. Seism. Soc. Am., 55, 463-486, 1965.

Wickens, A. J. and K. Pec, A crust-mantle profile from Mould Bay, Canada, to Tucson, Arizona, Bull. Seism. Soc. Am., 58, 1821-1831, 1968.

Appendix

```
C  A1 = SLOPE OF LEFT ASYMPTOTE
C  A2 = SLOPE OF RIGHT ASYMPTOTE
C  H = INTERVAL AT WHICH DATA ARE READ
C  A,B = LIMITS OF INTEGRATION(MUST BE SYMMETRICAL RELATIVE TO 0)
C  C,D = LIMITS OF AVAILABLE DATA ON BODE PLOT
C  W = ANGULAR FREQUENCY FOR WHICH WE SEEK PHASE RESPONSE
C  XW = LOG OF W
C  XMIN = LOG OF MINIMUM W
C  XMAX = LOG OF MAXIMUM W
C  NW = TOTAL NUMBER OF POINTS FROM A TO B
C  N = TOTAL NUMBER OF POINTS FROM C TO D
C  NT = TOTAL NUMBER OF POINTS FROM A+XMIN TO B+XMAX
C  L = TOTAL NUMBER OF POINTS FOR WHICH WE SEEK PHASE RESPONSE
C  A,B,C,D,XW MUST BE INTEGRAL MULTIPLES OF H, OTHERWISE LIMITS WILL NOT BE AT
C  DATA POINTS OR DERIVATIVE AND WEIGHTING FUNCTIONS WILL NOT LINE-UP WHEN SHIF-
C  TED RELATIVE TO EACH OTHER
C  IF ANY CONSTANT IS CHANGED IN THE PROGRAM ONLY THE FIRST PART MUST BE REVISED
C  DIMENSIONS ARE AS FOLLOWS: AMP(N), DER(N), DE(NT), WE(NW), XW(L), PHASE(L)
C
C  DETERMINATION OF THE CONSTANTS
C
      A1 = +4.
      A2= -2.
      H=0.2
      A = -7.
      B = +7.
      C = -4.
      D = +5.
      XMIN = -2.8
      XMAX = +2.
      N = (D-C)/H+1.1
      NT = ((B+XMAX)-(A+XMIN))/H+1.1
      NW = (B-A)/H+1.1
      L=25
      DIMENSION AMP(46), DER(46), DE(95), WE(71), XW(25), PHASE(25)
C
C  COMPUTATION OF THE DERIVATIVE
C
      READ(5,91) AMP
   91 FORMAT(13F6.2)
      M = N-1
      DER(1) = A1
      DO 15 I = 2,M
   15 DER(I) = (AMP(I+1)-AMP(I-1))/(2.*H)
      DER(N) = A2
      WRITE(6,8) DER
```

```
    8 FORMAT(//26X,'DER'/(20X,F10.2))
C
C
C   EXTENSION OF THE RANGE OF THE DERIVATIVE
C
      N1 = (C-(A+XMIN))/H+.1
      DO 25 J = 1,N1
   25 DE(J) = A1
      N2 = N1+1
      N3 = N1+N
      DO 30 J = N2,N3
      I = J-N1
   30 DE(J) = DER(I)
      N4 = N3+1
      DO 40 J = N4,NT
   40 DE(J) = A2
C
C
C   TABULATION OF THE WEIGHTING FUNCTION
C
      PI = 3.141593
      X = A
      DO 50 K = 1,NW
      WE(K) = 1./PI*ALOG(1./TANH(ABS(X/2.)))
   50 X = X+H
      WRITE(6,77)
   77 FORMAT('1'10X,'XW'13X,'F'15X,'T'13X,'PHASE')
C
C
C   SHIFTING AND COMPUTATION OF THE INTEGRAL
C
      READ(5,92) XW
   92 FORMAT(20F4.1)
      MW = NW-1
      KW = NW-3
      DO 5 I = 1,L
      JA = (XW(I)-XMIN)/H+1.1
      JO = JA+MW/2
      FA = (DE(JA)-DE(JO))*WE(1)
      EVEN = 0.
      ODD = 0.
      DO 65 K = 2,KW,2
      EVEN = EVEN+(DE(JA-1+K)-DE(JO))*WE(K)
   65 ODD = ODD+(DE(JA+K)-DE(JO))*WE(K+1)
      FMW = (DE(JA+NW-2)-DE(JO))*WE(MW)
      FB = (DE(JA+MW)-DE(JO))*WE(NW)
      PHASE(I) = (FA+4.*(EVEN+FMW)+2.*ODD+FB)*H*60./PI+DE(JO)*90.
      F=EXP(XW(I))/(2.*PI)
      T = 1./F
    5 WRITE(6,97) XW(I), F, T, PHASE(I)
   97 FORMAT(/F14.1,F16.4,2F16.2)
C
C
C   PLOTTING OF THE PHASE RESPONSE
C
```

```
      CALL PLOTS
      CALL AXIS(0.,1.,'LOG OF ANGULAR FREQUENCY',-24,8.,0.,-4.,1.)
      CALL AXIS(0.,0.,'PHASE RESPONSE (SPRENGNETHER: OMM)',33,10.,90.,-3
     10.,30.)
      DO 18 I = 1,L
      XW(I) = XW(I)+4.
   18 PHASE(I) = (PHASE(I)+30.)/30.
      CALL PLOT(XW(1),PHASE(1),+3)
      DO 20 I = 2,L
   20 CALL PLOT(XW(I),PHASE(I),+2)
      CALL PLOTND
      STOP
      END
```

```
ORY REQUIREMENTS 000E02 BYTES

TIME =        3.2  SECONDS
```